TECHNICAL MEMORANDUM

730

Tropospheric Chemistry in the Integrated Forecasting System of ECMWF

Johannes Flemming[1], Vincent Huijnen[3], Joaquim Arteta[2], Peter Bechtold[1], Anton Beljaars[1], Anne-Marlene Blechschmidt[5], Michail Diamantakis[1],Richard J. Engelen[1],Audrey Gaudel[7],Antje Inness[1],Luke Jones[1],Eleni Katragkou[6], Vincent-Henri Peuch[1],Andreas Richter[5],Martin G. Schultz[4], Olaf Stein[4] and Athanasios Tsikerdekis[6]

Research Department

September 2014

1) European Centre for Medium-Range Weather Forecasts, Reading, UK
2) Météo-France, Toulouse, France
3) Royal Netherlands Meteorological Institute, De Bilt, The Netherlands
4) Institute for Energy and Climate Research, FZ Jülich, Germany
5) Universität Bremen, Germany
6) Aristotle University of Thessaloniki, Greece
7) CNRS, Laboratoire d'Aérologie, UMR 5560, Toulouse, France

European Centre for Medium-Range Weather Forecasts
Europäisches Zentrum für mittelfristige Wettervorhersage
Centre européen pour les prévisions météorologiques à moyen

Series: ECMWF Technical Memoranda

A full list of ECMWF Publications can be found on our web site under:
http://www.ecmwf.int/publications/

Contact: library@ecmwf.int

European Centre for Medium Range Weather Forecasts
Shinfield Park, Reading, Berkshire RG2 9AX, England

Abstract

A representation of atmospheric chemistry has been included in the Integrated Forecasting System (IFS) of the European Centre for Medium-range Weather Forecasts (ECMWF). The new chemistry modules complement the aerosol module of the IFS for atmospheric Composition, which is named C-IFS. C-IFS for chemistry supersedes a coupled system, in which the chemical transport model MOZART 3 was two-way coupled to the IFS (IFS-MOZART). This paper contains a description of the new on-line implementation, an evaluation with observations and a comparison of the performance of C-IFS with IFS-MOZART. The chemical mechanism of C-IFS is an extended version of the CB05 chemical mechanism as implemented TM5 model and a parameterization for stratospheric ozone. CB05 describes tropospheric chemistry with 54 species and 126 reactions. Wet deposition and lightning NO emissions are modelled in C-IFS using the detailed input of the IFS physics package. A one-year simulation for 2008 at a horizontal resolution of about 80 km is evaluated against ozone sondes, CO MOZAIC profiles, surface observations of ozone, CO, SO_2 and NO_2 as well as satellite retrievals of CO, tropospheric NO_2 and formaldehyde. MACCity anthropogenic emissions and biomass burning emissions from the GFAS data set were used in the simulation. C-IFS (CB05) showed an improved performance with respect to MOZART for CO, winter-time SO_2 and upper tropospheric ozone and was of a similar accuracy for the other evaluated species. C-IFS (CB05) is about ten times more computationally efficient than IFS-MOZART.

1 Introduction

Monitoring and forecasting of global atmospheric composition are key objectives of the atmosphere service of the European Copernicus Programme. The Copernicus Atmosphere Monitoring Service (CAMS) is based on combining satellite observations of atmospheric composition with state-of-the-art atmospheric modelling (Flemming et al., 2013 and Hollingsworth et al., 2008). For that purpose, ECMWF's numerical weather prediction (NWP) system, the IFS, was extended for forecast and assimilation of atmospheric composition. Modules for aerosols (Morcrette et al., 2009, Benedetti et al., 2009) and greenhouse gases (Engelen et al., 2009) were integrated on-line in the IFS. Because of the complexity of the chemical mechanisms for reactive gases, modules for atmospheric chemistry were not initially included in the IFS. Instead a coupled system (Flemming et al., 2009a) was developed, which couples the IFS to the chemical transport models (CTM) MOZART 3.5 (Kinnison et al., 2007) or TM5 (Huijnen et al., 2010) by means of the OASIS4 coupler software (Redler et al., 2010). Van Noije et al. (2014) coupled TM5 to IFS for climate applications in a similar approach. The coupled system IFS-CTM made it possible to assimilate satellite retrievals of reactive gases with the assimilation algorithm of the IFS, which is also used for the assimilation of meteorological observations as well as for aerosol and greenhouse gases. The building block of CAMS are currently run in pre-operational mode as part of the Monitoring Atmospheric Composition and Climate - Interim Implementation project (MACC II).

The coupled system IFS-MOZART has been successfully used for a re-analysis of atmospheric composition (Inness et al., 2013), pre-operational atmospheric composition forecasts (Stein et al., 2012), forecast and assimilation of the stratospheric ozone (Flemming et al., 2011a,, Lefever et al., 2014) and tropospheric CO (Eligundi et al., 2010) and ozone (Ordonez et al., 2010). The coupled system IFS-TM5 has been used in a case study on a period with intense biomass burning in Russia in 2010 (Huijnen et al., 2012). Nevertheless, the coupled approach has limitation such as the need for interpolation between the IFS and CTM model grids and the duplicate simulation of transport processes. Further, its computational performance is often not optimal as it can suffer from load imbalances between the coupled components.

Consequently, modules for atmospheric chemistry and related physical processes have now been integrated on-line in the IFS, thereby complementing the on-line integration strategy already pursued for aerosol and greenhouse gases in IFS. The IFS including modules for atmospheric composition is named Composition-IFS (C-IFS). C-IFS makes it possible (i) to use the detailed meteorological simulation of the IFS for the simulation of the fate of constituents (ii) to use the IFS data assimilation system to assimilate observations of atmospheric composition and (iii) to simulate feedback processes between atmospheric composition and weather. A further advantage of C-IFS is the possibility of model runs at a high horizontal and vertical resolution because of the high computational efficiency of C-IFS.

Including chemistry modules in general circulation models (GCM) started in the mid-1990 to simulate interaction of stratospheric ozone (e.g. Steil et al., 1998) and aerosols (e.g. Haywood et al.1997) in the climate system. Later, the more comprehensive schemes for tropospheric chemistry were included in climate GCM such as ECHAM5-HAMMOZ (Pozzoli et al., 2008; Rast et al., 2014) and CAM-chem (Lamarque et al., 2012) to study short-lived greenhouse gases and the influence of climate change on air pollution (e.g. Fiore et al., 2010). Examples of the on-line integration of chemistry modules in global circulation models with focus on NWP are GEM-AQ (Kaminski et al., 2008), GEMS-BACH

(Menard et al., 2007) and WRF/Chem (Grell et al., 2005). In the UK Met Office's Unified Model stratospheric chemistry (Morgenstern et al., 2009) and tropospheric chemistry (O'Connor et al., 2014) can be simulated together with the GLOMAP mode aerosol scheme (Mann et al., 2010). Baklanov et al. (2014) give an overview of on-line coupled chemistry-meteorological models for regional applications.

C-IFS is intended to run with several chemistry schemes for both the troposphere and the stratosphere in the future. Currently, only the tropospheric chemical mechanism CB05 originating from the TM5 CTM (Huijnen et al., 2010) has been thoroughly tested. For example, C-IFS (CB05) has been applied to study the HO_2 uptake on clouds and aerosols (Huijnen, Williams and Flemming, 2014) and pollution in the Artic (Emmons et al., in prep). The tropospheric and stratospheric scheme RACMOBUS of the MOCAGE model (Bousserez et al., 2007) and the MOZART 3.5 chemical scheme as well as an extension of the CB05 scheme with the stratospheric chemical mechanism of the BASCOE model (Errera et al., 2008) have been technically implemented and are being scientifically tested. Only C-IFS (CB05) is the subject of this paper.

Each chemistry scheme in C-IFS consists of the specific gas phase chemical mechanism, multi-phase chemistry, the calculation of photolysis rates and upper chemical boundary conditions. The newly developed routines for dry and wet deposition, emission injection, parameterization of lightning NO_X emissions as well as transport and diffusion are simulated by the same approach for all chemistry schemes. Likewise, emissions and dry deposition input data are kept the same for all configurations.

The purpose of this paper is to document C-IFS and to present its model performance with respect to observations. Since it foreseen that C-IFS (CB05) replaces the current operational MACC model system for reactive gases (IFS-MOZART) both in data assimilation and forecast mode, the evaluation in this paper is carried out predominately with observations that are used for the routine evaluation of the MACC II system. The model results are compared (i) with a MOZART simulation, which produces very similar results as IFS-MOZART in forecast mode, and (ii) with the MACC re-analysis (Inness et al., 2013), which is an application of IFS-MOZART in data assimilation mode. All model configurations used the same emission data. The comparison demonstrates that C-IFS is ready to be used operationally.

The paper is structured as follows. Section 2 is a description of the C-IFS, with focus on the newly implemented physical parameterizations and the chemical mechanism CB05. Section 3 contains the evaluation with observations of a one year simulation with C-IFS (CB05) and a comparison with the results from the MOZART run and the MACC re-analysis. The paper is concluded with a summary and an outlook in section 4.

2 Description of C-IFS

2.1 Overview of C-IFS

The IFS consists of a spectral NWP model that applies the semi-Lagrangian semi-implicit method to solve the governing dynamical equations. The simulation of the hydrological cycle includes prognostic representations of cloud fraction, cloud liquid water, cloud ice, rain and snow (Forbes et al., 2011). The simulations presented in this paper used the IFS release CY40r1. The technical and scientific documentation of this IFS release can be found at

http://www.ecmwf.int/research/ifsdocs/CY40r1/index.html. Changes of the operational model are documented on https://software.ecmwf.int/wiki/display/IFS/Operational+changes.

At the start of the time step, the three-dimensional advection of the tracers mass mixing ratios is simulated by the semi-Lagrangian method as described in Temperton, Hortal and Simmons (2001) and Hortal (2002). Next, the tracers are vertically distributed by the diffusion scheme (Beljaars et al., 1998) and by convective mass fluxes (Bechtold et al., 2014). The diffusion scheme also simulates the injection of emissions and the loss by dry deposition. The output of the convection scheme is used to calculate NO production by lightning. Finally, the sink and source terms due to chemical conversion, wet deposition and prescribed surface and stratospheric boundary conditions (CH_4 and HNO_3) are calculated.

The chemical species and the related processes are represented only in grid-point space. The horizontal grid is a reduced Gaussian grid (Hortal and Simmons, 1991). C-IFS can be run at varying vertical and horizontal resolutions. The simulations presented in this paper were carried out at a T255 spectral resolution (i.e. truncation at wavenumber 255), which corresponds to a grid box size of about 80 km. The vertical discretization uses 60 levels up to the model top at 0.1 hPa (65 km) in a hybrid sigma-pressure coordinate. The vertical extent of the lowest level is about 17 m; it is 100 m at about 300m above ground, 400-600 m in the middle troposphere and about 800 m at about 10 km height.

The modus operandi of C-IFS is one of a forecast model in a NWP framework. The simulations of C-IFS are a sequence of daily forecasts over a period of several days. Each forecast is initialised by the ECMWF's operational analysis for the meteorological fields and by the 3D chemistry fields from the previous forecast ("forecast mode"). Continuous simulations over longer periods are carried out in "relaxation mode". In relaxation mode the meteorological fields are relaxed to the fields of a meteorological re-analysis, such as ERA-Interim, during the run (Jung et al., 2008) to ensure realistic and consistent meteorological fields.

2.2 Transport

The transport by advection, convection and turbulent diffusion of the chemical tracers uses the same algorithms as developed for the transport of water vapor in the NWP applications of IFS. The advection is simulated with a three-dimensional semi-Lagrangian advection scheme, which applies a quasi-montonic cubic interpolation of the departure values. Since the semi-Lagrangian advection does not formally conserve mass a global mass fixer is applied. The effect of different global mass fixers is discussed in Diamantakis and Flemming (2014) and Flemming and Huijnen (2011 b). The mass fixer according to McGregor (2005) was used for the runs presented in this paper because of the overall best balance between the results and computational cost.

The vertical turbulent transport in the boundary layer is represented by a first order K-diffusion closure. The surface emissions are injected as lower boundary flux in the diffusion scheme. The lower boundary flux condition also accounts for the dry deposition flux based on the projected surface mass mixing ratio in an implicit way. The vertical transport by convection is simulated as part of the cumulus convection. It applies a bulk mass flux scheme which was originally described in Tiedtke (1989). The scheme considers deep, shallow and mid-level convection. Clouds are represented by a single pair of entraining/detraining plumes which determine the updraught and downdraught mass fluxes. (http://old.ecmwf.int/research/ifsdocs/CY40r1/ in Physical Processes, Chapter 6, pp 73-90).

Highly soluble species such as HNO_3, H_2O_2 and aerosol precursors are assumed to be scavenged in the convective rain droplets and are therefore excluded from the convective mass transfer.

The operator splitting between the transport and the sink and source terms follows the implementation for water vapour (Beljaars et al., 2004). Advection, diffusion and convection are simulated sequentially. The sink and source processes are simulated in parallel using an intermediate update of the mass mixing ratios with all transport tendencies. At the end of the time step tendencies from transport and sink and source terms are added together for the final update the concentration fields. Resulting negative mass mixing ratios are corrected at this point by setting the updated mass mixing ratio to a "chemical zero" of 1.0e-25 kg/kg.

2.3 Emissions for 2008

The anthropogenic surface emissions were given by the MACCity inventory (Granier et al., 2011) and aircraft NO emissions of a total of ~0.8 Tg N/yr were applied (Lamarque et al, 2010). Natural emissions from soils and oceans were taken from the POET database for 2000 (Granier et al., 2005; Olivier et al., 2003). The biogenic emissions were simulated by the MEGAN2.1 model (Guenther et al., 2006). Biomass burning emissions were produced by the Global Fire Assimilation System (GFAS) version 1, which is based on satellite retrievals of fire radiative power (Kaiser et al., 2012). The actual emission totals used in the T255 simulation for 2008 from anthropogenic, biogenic sources and biomass burning as well as lighting NO are given in Table 1.

Species	Anthropogenic	Biogenic and natural	Biomass burning
CO	584	96	325
NO	70.2 + 1.8	10.7	9.2 + 12.3 (LiNO)
HCHO	3.4	4.0	4.9
CH_3OH	2.2	159	8.5
C_2H_6	3.4	1.1	2.3
C_2H_5OH	3.1	0	0
C_2H_4	7.7	18.0	4.3
C_3H_8	4.0	1.3	1.2
C_3H_6	3.5	7.6	2.5
PAR (Tg C)	30.9	18.1	1.7
OLE (Tg C)	2.4	0.0	0.7
ALD2 (Tg C)	1.1	6.1	2.17
CH_3COCH_3	1.3	28.5	2.4
Isoprene	0	523	0
Terpenes	0	97	0
CH_4	483 total		

Table 1 Annual emissions from anthropogenic, biogenic and natural sources and biomass burning for 2008 in Tg for a C-IFS (CB05) run at T255 resolution. CH_4 emissions are estimated from the contribution of the prescribed mass mixing ratio in the surface layer. Anthropogenic NO emissions contain a contribution of 1.8 Tg aircraft emissions and 12.3 Tg (5.7 Tg N) lightning emissions (LiNO) is added in the biomass burning columns.

2.4 Physical parameterizations of sources and sinks

2.4.1 Dry deposition

Dry deposition is an important removal mechanism at the surface in the absence of precipitation. It depends on the diffusion close to the earth surface, the properties of the constituent and on the characteristics of the surface, in particular the type and state of the vegetation and the presence of intercepted rain water. Dry deposition plays an important role in the biogeochemical cycles of nitrogen and sulphur, and it is a major loss process of tropospheric ozone. Modelling the dry deposition fluxes in C-IFS is based on a resistance model (Wesely et al., 1989), which differentiates the aerodynamic, the quasi-laminar and the canopy or surface resistance. The inverse of the total resistance is equivalent to a dry deposition velocity V_D.

The dry deposition flux F_D at the model surface is calculated based on the dry deposition velocity V_D, the mass mixing ratio X_s and air density ρ at the lowest model level *s,* in the following way:

$$F_D = V_D \, X_S \, \rho_S$$

The calculation of the loss by dry deposition has to account for the implicit character of the dry deposition flux since it depends on the mass mixing ratio X_s. itself

The dry deposition velocities were calculated as monthly mean values from a one-year simulation using the approach described in Michou et al. (2004). It used meteorological and surface input data such as wind speed, temperature surface roughness and soil wetness from the ERA-interim data set. At the surface the scheme makes a distinction between uptake resistances for vegetation, bare soil, water, snow and ice. The surface and vegetation resistances for the different species are calculated using the stomatal resistance of water vapour. The stomatal resistance for water vapour is calculated depending on the leaf area index, radiation and the soil wetness at the uppermost surface layer. Together with the cuticlular and mesophyllic resistances this is combined into the leaf resistance according to Wesely et al. (1989) using season and surface type specific parameters as referenced in Seinfeld and Pandis (1998).

Dry deposition velocities have higher values during the day because of lower aerodynamic resistance and canopy resistance. Zhang et al. (2003) reported that averaged observed ozone and SO_2 dry deposition velocities can be up to 4 times higher at day time than at night time. As this important variation is not captured with the monthly-mean dry deposition values, a +/- 50% variation is imposed on all dry deposition values based on the cosine of the solar zenith angle. This modulation tends to decrease dry deposition for species with a night time maximum at the lowest model level and it increases dry deposition of ozone.

Table A4 (supplement) contains annual total loss by dry deposition and expressed as a life-time estimate by dividing by tropospheric burden for a simulation using monthly dry deposition values for 2008. Dry deposition was most effective for many species in particular SO_2 and NH_3 as the respective lifetimes were one day to one week. For tropospheric ozone the respective globally averaged time scale is about 3 months. Because dry deposition occurs mainly over ice-free land surfaces the corresponding time scale is at least three times shorter in these areas.

2.4.2 Wet Deposition

Wet deposition is the transport of soluble or scavenged constituents by precipitation. It includes the following processes:

- In-cloud scavenging and removal by rain and snow (rain out)
- Release by evaporation of rain and snow
- Below cloud scavenging by precipitation falling through without formation of precipitation (wash out)

It is important to take the sub-grid scale of cloud and precipitation-formation into account for the simulation of wet deposition. The IFS cloud scheme provides information on the cloud and the precipitation fraction for each grid box. It uses a random overlap assumption (Jakob and Klein, 2000) to derive cloud and precipitation area fraction. The same method has been used by Neu and Prather (2012), who demonstrated the importance of the overlap assumption for the simulation of the wet deposition. The precipitation fluxes for the simulation of wet removal in C-IFS were scaled to be valid over the precipitation fraction of the respective grid-box. The loss of tracer by rain-out and wash-out was limited to the area of the grid box covered by precipitation. Likewise, the cloud water and ice content is scaled to the respective cloud area fraction. If the sub-grid scale distribution was not considered in this way, wet deposition was lower for highly soluble species such as HNO_3 because the species is only removed from the cloudy or rainy grid box fraction. For species with low solubility the wet deposition loss was slightly decreased because of the decrease in effective cloud and rain water.

Even if wet deposition removes tracer mass only in the precipitation area, the mass mixing ratio representing the entire grid box is changed accordingly after each model time step. This is equivalent with the assumption that there is instantaneous mixing within the grid-box at the time scale of the model time step. As discussed in Huijnen, Williams and Flemming (2014), this assumption may lead to an overestimation of the simulated tracer loss.

The module for wet deposition in C-IFS is based on the Harvard wet deposition scheme (Jacob et al., 2000 and Liu et al., 2001). In contrast to Jacob et al. (2000), tracers scavenged in wet convective updrafts are not removed as part of the convection scheme. Nevertheless, the fraction of highly soluble tracers in cloud condensate is simulated to limit the amount of tracers lifted upwards as only the gas phase fraction is transported by the mass flux. The removal by convective precipitation is simulated in the same way as for large-scale precipitation in the wet deposition routine.

The input fields to the wet deposition routine are the following prognostic variables, calculated by the IFS cloud scheme (Forbes et al., 2011): total cloud and ice water content, grid-scale rain- and snow water content and cloud and grid-scale precipitation fraction as well as the derived fluxes for convective and grid-scale precipitation fluxes at the grid cell interfaces. For convective precipitation a precipitation fraction of 0.05 is assumed and the convective rain and snow water content is calculated assuming a droplet fall speed of 5 m/s.

Wash-out, evaporation and rain-out are calculated after each other for large-scale and convective precipitation. The amount of trace gas dissolved in cloud droplets is calculated using Henrys-law-equilibrium or assuming that 70% of the aerosol precursors (SO_4, NH_3 and NO_3) is dissolved in the droplet. The effective Henry coefficient for SO_2, which accounts for the dissociation of SO_2, is

calculated following Seinfeld and Pandis (1998, p. 350). The other Henry's law coefficients are taken from the compilation by Sander 1999 (www.henrys-law.org, Table A1 in the supplement).

The loss by rain out is determined by the precipitation formation rate. The retention coefficient R, which accounts for the retention of dissolved gas in the liquid cloud condensate as it is converted to precipitation, is one for all species in warm clouds (T > 268 K). For mixed clouds (T < 268 K) R is 0.02 for all species but 1.0 for HNO_3 and 0.6 for H_2O_2 (von Blohn, 2011). In ice clouds only H_2O_2 (Lawrence and Crutzen, 1998) and HNO_3 are scavenged.

Partial evaporation of the precipitation fluxes leads to the release of 50% of the resolved tracer and 100% in the case of total evaporation (Jacobs et al., 2000). Wash-out is either mass-transfer or Henry-equilibrium limited. HNO_3, aerosol precursors and other highly soluble gases are washed out using a first order wash-out rate of 0.1 mm^{-1} to account for the mass transfer. For less soluble gases the resolved fraction in the rain water is calculated assuming Henry equilibrium in the evaporated precipitation.

Table A5 (supplement) contains total loss by wet deposition and expressed as time scale in days based on the tropospheric burden. For aerosol precursors nitrate, sulphate and ammonium, HNO_3 and H_2O_2 wet deposition is the most important loss process with respective timescales of 2–4 days.

2.4.3 NO emissions from lightning

NO emissions from lightning are a considerable contribution to the global atmospheric NO_x budget. Estimates of the global annual source vary between 2–8 Tg (N) yr−1 (Schumann and Huntrieser, 2007). 5 Tg(N) (10.7 Tg NO) is the most commonly assumed value for global CTMs which is about 6-7 times the value of NO emissions from aircraft (Gauss et al., 2006) or 17% of the total anthropogenic emissions. NO emissions from lightning play an important role in the chemistry of the atmosphere because they are released in the rather clean air of the free troposphere, where they can strongly influence the ozone budget and hence the OH-HO_2 partitioning.

The parameterization of the lightning NO production C-IFS consist of estimates of (i) the flash rate density, (ii) the flash energy release and (iii) the vertical emission profile for each model grid column. The estimate of the flash-rate density is based on parameters of the convection scheme. The C-IFS has two options to simulate the flash-rate densities using the following input parameters: (i) convective cloud height (Price and Rind, 1992) or (ii) convective precipitation (Meijer et al., 2001).

The parameterizations distinguish between land and ocean points by assuming about 5-10 times higher flash rates over land. Additional checks on cloud base height, cloud extent and temperature are implemented to select only clouds that are likely to generate lightning strokes. The coefficients of the two parameterizations were derived from field studies and depend on the model resolution. With the current implementation of C-IFS (T255L60), the global flash rates were 26 and 43 flashes per seconds for the schemes by Price and Rind (1992) and Meijer et al. (2001), respectively. It seemed therefore necessary to scale the coefficients to get a flash rate in the range of the observed values of about 40-50 flashes per second derived from LIS/OTD observations (Cecil et al., 2012). Figure 1 shows the annual flash rate density simulated by the two parameterisations together with observations from the LIS/OTD data set. The two approaches show the main flash activity in the tropics but there are differences in the distributions over land and sea. The smaller land - seas differences of Meijer et al. (2001) agreed better with the observations. The observed maximum over Central African was well reproduced by both parameterizations but the schemes produce an exaggerated maximum over tropical

South America. The lightning activity of the US underestimated. The parameterization by Meijer et al. (2001) has been used for the C-IFS runs presented in this paper.

Cloud to ground (CG) and cloud to cloud (CC) flashes are assumed to release a different amount of energy, which is proportional to the NO release. Price et al. (1997) suggest that the energy release of CG is 10 times higher. However, more recent studies suggest a similar value for CG and CC energy release based on aircraft observations and model studies (Ott et al., 2010), which we follow in C-IFS. In C-IFS, CG and CC fractions are calculated using the approach by Price and Rind (1993), which is based on a 4th order function of cloud height above freezing level.

The vertical distribution of the NO release is of importance for its impact on atmospheric chemistry. Many CTMs use the suggestion of Pickering et al. (1998) of a C-shape profile, which peaks at the surface and in the upper troposphere. Ott et al. (2010) suggest a "backward C-shape" profile which locates most of the emission in the middle of the troposphere. The vertical distribution can be simulated by C-IFS (i) according to Ott et al. (2010) or (ii) in version of the C-shape profile following Huijnen et al. (2010). The approach by Ott et al. (2010) is used in the simulation presented here.

As the lightning emissions depend on the convective activity they change at different resolutions or after changes to the convection scheme. The C-IFS lightning emissions were 4.9 Tg (N) at T159 resolution and 5.7 Tg (N) at T255 resolution.

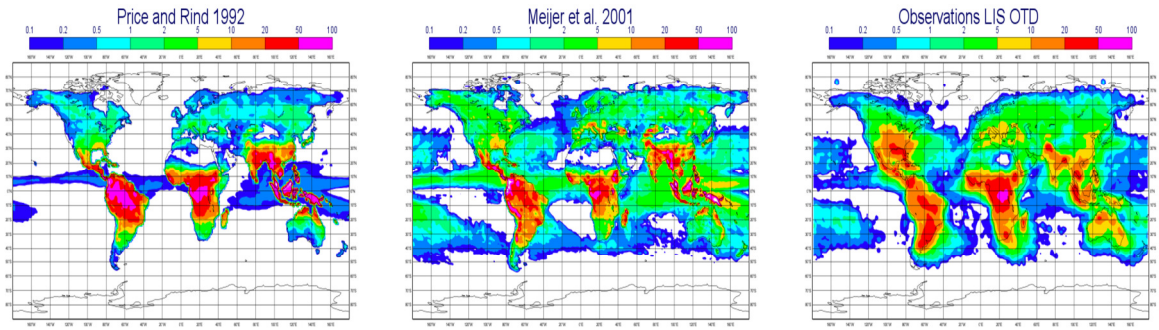

Figure 1 Flash density in flashes/(km^2 yr) from the IFS input data using the parameterization by Price and Rind (1992) (left), Meijer et al. (2001) (middle) and observations from the LIS OTD data base (right). All fields were scaled to an annual flash density of 46 fl/s.

2.5 CB05 chemistry scheme

2.5.1 Gas-phase chemistry

The chemical mechanism is a modified version of the Carbon Bond mechanism 5 (CB05, Yarwood et al., 2005), which is originally based on the work of Gery et al. (1989) with added reactions from Zaveri and Peters (1999) and from Houweling et al. (1998) for isoprene. The CB05 scheme adopts a lumping approach for organic species by defining a separate tracer species for specific types of functional groups. The speciation of the explicit species into lumped species follows the recommendations given in Yarwood et al. (2005). The CB05 scheme used in C-IFS has been further extended in the following way: An explicit treatment of methanol (CH_3OH), ethane (C_2H_6), propane (C_3H_8), propene (C_3H_6) and acetone (CH_3COCH_3) has been introduced as described in Williams et al., (2013). The isoprene oxidation has been modified motivated by Archibald et al. (2010). Higher C3

peroxy-radicals formed during the oxidation of C_3H_6 and C_3H_8 were included following Emmons et al. (2010).

The CB05 scheme is supplemented with chemical reactions for the oxidation of SO_2, di-methyl sulphide (DMS), methyl sulphonic acid (MSA) and ammonia (NH_3), as outlined in Huijnen, Williams and Flemming (2014). For the oxidation of DMS, the approach of Chin et al. (1996) is adopted. Table A1 (supplement) gives a comprehensive list of the trace gases included in the chemical scheme.

The reaction rates have been updated according to the recommendations given in either Sander et al. (2011) or Atkinson et al. (2004, 2006). The oxidation of CO by OH implicitly accounts for the formation and subsequent decomposition of the intermediate species HOCO as outlined in Sander et al. (2006). For lumped species, e.g. ALD2, the reaction rate is determined by an average of the rates of reaction for the most abundant species, e.g. C2 and C3 aldehydes, in that group. An overview of all gas-phase reactions and reaction rates as applied in this version of C-IFS can be found in Table A2 (supplement).

For the loss of trace gases by heterogeneous oxidation processes, the model explicitly accounts for the oxidation of SO_2 in cloud through aqueous phase reactions with H_2O_2 and O_3, depending on the acidity of the solution. In this version of C-IFS, heterogeneous conversion of N_2O_5 into HNO_3 on cloud droplets and aerosol particles is applied with a reaction probability (γ) set to 0.02 (Huijnen, Williams and Flemming, 2014).

2.5.2 Photolysis rates

For the calculation of photo-dissociation rates an on-line parameterization for the derivation of actinic fluxes is used (Williams et al., 2012, 2006). It applies a Modified Band Approach (MBA) which is an updated version of the work by Landgraf and Crutzen (1998), tailored and optimized for use in tropospheric CTMs. The approach uses 7 absorption bands across the spectral range 202 – 695 nm. At instances of large solar zenith angles (71-85°) a different set of band intervals is used. In the MBA the radiative transfer calculation using the absorption and scattering components introduced by gases, aerosols and clouds is computed on-line for each of 7 pre-defined band intervals based on the 2-stream solver of Zdunkowski et al. (1980). Mie-scattering components introduced by both clouds and aerosols can be accounted for.

The optical depth of clouds is calculated based on a parameterization available in IFS (Slingo, 1989 and Fu et al., 1996) for the cloud optical thickness at 550 nm. For the simulation of the impact of aerosols on the photolysis rates a climatological field for aerosols is used, as detailed in Williams et al. (2012). There is also an option to use the MACC aerosol fields.

In total 20 photolysis rates are included in the scheme, as given in Table A3 (supplement). The explicit nature of the MBA implies a good flexibility in terms of updating molecular absorption properties (cross sections and quantum yields) and the addition of new photolysis rates into the model.

2.5.3 The chemical solver

The chemical solver used in C-IFS (CB05) is an Euler Backward Iterative (EBI) solver (Hertel et al., 1996). This solver has been originally designed for use with the CBM4 mechanism of Gery et al. (1989). The chemical time step is 22.5 min, which is half of the dynamical model time step of 45 min

at T255 resolution. Eight, four or one iterations are carried out for fast-, medium- and slow-reacting chemical species to obtain a solution. The number of iterations is doubled in the lowest four models levels, where the perturbations due to emissions can be large.

2.5.4 Stratospheric boundary conditions

The modified CB05 chemical mechanism includes no halogenated species and no photolytic destruction below 202 nm and is therefore not suited for the description of stratospheric chemistry. Thus realistic upper boundary conditions for the longer-lived gases such as O_3, CH_4, and HNO_3 are needed to capture the influence of stratospheric intrusions on the composition of the upper troposphere.

Stratospheric O_3 chemistry in C-IFS CB05 is parametrised by the Cariolle scheme (Cariolle and Teyssèdre, 2007). Chemical tendencies for stratospheric and tropospheric O_3 are merged at an empirical interface of the diagnosed tropopause height in IFS. Additionally, stratospheric ozone in C-IFS can be nudged to ozone analyses of either the MACC re-analysis (Inness et al., 2013) or ERA interim (Dee et al., 2011). The tropopause height in IFS is diagnosed either form the gradient in humidity or the vertical temperature gradient.

For HNO_3 a stratospheric climatology based on the UARS MLS satellite observations is applied by prescribing the ratio of HNO_3/O_3 at 10 hPa. Further, stratospheric CH_4 is constraint by a climatology based on HALOE observations (Grooß and Russel, 2005), at 45hPa (and 90 hPa in the extra-tropics) which implicitly accounts for the stratospheric chemical loss of CH_4 by OH, Cl and $O(^1D)$. It should be noted that also the surface concentrations of CH_4 are fixed in this configuration of the model.

2.5.5 Gas-aerosol partitioning

Gas-aerosol partitioning is calculated using the Equilibrium Simplified Aerosol Model (EQSAM, Metzger et al., 2002a, 2002b). The scheme has been simplified so that only the partitioning between HNO_3 and the nitrate aerosol (NO^-_3) and between NH_3 and the ammonium aerosol (NH^+_4) is calculated. SO^{2-}_4 is assumed to remain completely in the aerosol phase because of its very low vapour pressure. The assumptions of the equilibrium model are that (i) aerosols are internally mixed and obey thermodynamic gas/aerosol equilibrium and that (ii) the water activity of an aqueous aerosol particle is equal to the ambient relative humidity (RH). Furthermore, the aerosol water mainly depends on the aerosol mass and the type of the solute, so that parameterizations of single solute molalities and activity coefficients can be defined, depending only on the type of the solute and RH. The advantage of using such parameterizations is that the entire aerosol equilibrium composition can be solved analytically. For atmospheric aerosols in thermodynamic equilibrium with the ambient RH, the following reactions are considered in C-IFS. The subscripts g, s and aq denote gas, solid and aqueous phase, respectively:

$$(NH_3)_g + (HNO_3)_g \leftrightarrow (NH_4NO_3)_s$$

$$(NH_4NO_3)_s + (H_2O)_g \leftrightarrow (NH_4NO_3)_{aq} + (H_2O)_{aq}$$

$$(NH_4NO_3)_{aq} + (H_2O)_g \leftrightarrow (NH^+_4)_{aq} + (NO^-_3)_{aq} + (H_2O)_{aq}$$

2.6 Model budget diagnostics

C-IFS computes global diagnostics for every time step to study the contribution of different processes on the global budget. The basic outputs are the total and tropospheric tracer mass, the global integral of the total emissions, integrated wet and dry deposition fluxes, chemical conversion as well as atmospheric emissions and the contributions of prescribed upper and lower vertical boundary conditions for CH_4 and HNO_3. A time-invariant pressure-based tropopause definition is used to calculate the tropospheric mass. To monitor the numerical integrity of the scheme, the contributions of the corrections to ensure positiveness and global mass conservation are calculated. Optionally, more detailed diagnostics can be requested that includes photolytic loss and the loss by OH for the tropics and extra-tropics.

A detailed analysis of the global chemistry budget is beyond the scope of this paper. Only a number of key terms for CO, ozone and CH_4 is summarized here. They are compared with values from the ACCENT model inter-comparisons of climate CTM reported by Stevenson et al. (2006) for tropospheric ozone and by Shindell et al. (2006) for CO. A more recent inter-comparison was carried out within the ACCMIP activities. The ACCMIP values have been taken from Young et al. (2012) for tropospheric ozone and from Voulgarakis et al. (2013) for methane. It should be noted that the values from these inter-comparison are valid for present-day conditions but not specifically for 2008. A further source of the differences is the height of the tropopause assumed in the calculations. Overall, the comparison showed that the C-IFS (CB05) is well within the range of the other CTM.

The annual mean of C-IFS tropospheric ozone burden was 388 Tg. The values are at the upper end of the range simulated by the ACCENT (344 ± 39 Tg) and the ACCMIP (337 ± 23 Tg) CTMs. The same holds for the loss by dry deposition, which was 1158 Tg/yr for C-IFS, 1003 ± 200 Tg/yr for ACCENT and in the range 687-1350 Tg/yr for ACCMIP. The tropospheric chemical ozone production of C-IFS was 4618 Tg/yr and loss 4149 Tg/yr, which is for both values at the lower end of the range reported for the production (5110 ± 606 Tg/yr) and loss (4668 ± 727 Tg/yr) for the ACCENT models. Stratospheric inflow in C-IFS, estimated as the residue from the remaining terms was 689 Tg and the corresponding value from the ACCENT multi-model mean is 552 ± 168 Tg.

The annual mean total CO burden in C-IFS was 361 Tg, which is slightly higher than the ACCENT mean (345 Tg, 248-427 Tg). The total CO emissions in 2008 were 1005 Tg which is in-line with the number used in ACCENT (1077 Tg/yr) but lower than the estimate of IPCC TAR (1550 Tg/yr Smithson, 2002), which also takes into account results from inverse modelling studies. The tropospheric chemical CO production was 1410 Tg, which is close to the ACCENT multi-mean of 1505 +/- 236 Tg/yr. The chemical CO loss in C-IFS was 2050 Tg and the loss by dry deposition 23 Tg.

The annual mean CH_4 global and tropospheric burdens of C-IFS (CB05) are 4870 and 4270 Tg, respectively. The global chemical CH_4 loss by OH was 490 Tg/yr. Following Stevenson et al. (2006), this leads to a global CH_4 lifetime estimate of 9.2 yr. This value is within the ACCMIP range of 9.8±1.6 yr but lower than an observation-based 11.2±1.3 yr estimate by Prather et al., 2012. Methane emissions were substituted by prescribed monthly zonal-mean surface concentrations to avoid the long-spin up needed by a direct modeling of the methane surface fluxes. The resulting effective methane emissions were 483 Tg, which is of similar size as the sum of current estimates of the total methane emissions of 500 - 580 Tg and the loss by soils of 30-40 Tg (IPCC AR4 http://www.ipcc.ch/publications_and_data/ar4/wg1/en/ch7s7-4-1.html#ar4top).

3 Evaluation with observations and comparison with the coupled system IFS-MOZART

The main motivation for the development of C-IFS is forecasting and assimilation of atmospheric composition as part of the CAMS. Hence, the purpose of this evaluation is to show how C-IFS (CB05) performs with respect to the coupled CTM MOZART-3 (Kinnison et al., 2007), which has been running in the coupled system IFS-MOZART in pre-operational mode since 2007. C-IFS will replace the coupled system in the next update of the CAMS system. The evaluation focuses on species which are relevant to global air pollution such as tropospheric ozone, CO, NO_2, SO_2 and HCHO. The MACC re-analysis (Inness et al., 2013), which is an application of IFS-MOZART with assimilation of observations of atmospheric composition, has been included in the evaluation as a benchmark.

The MACC re-analysis (REAN) and a corresponding MOZART (MOZ) stand-alone run have been evaluated with observations by Inness et al. (2013). Further, the MACC-II sub-project on validation has compiled a comprehensive report assessing this data set (MACC, 2013). REAN has been further evaluated with surface observations in Europe and North-America for ozone by Im et al. (2014, submitted) and by Giordano et al. (2014, submitted) for CO. C-IFS (CB05) has been already evaluated with special focus on HO_2 in relation to CO in Huijnen, Williams and Flemming (2014). The performance of an earlier version of C-IFS (CB05) in the Arctic was evaluated and inter-compared with CTMs of the POLMIP project by Monks et al. (2014, submitted) for CO and Arnold et al. (2014, submitted) for reactive nitrogen. The POLMIP inter-comparisons show that C-IFS (CB05) performs within the range of other state-of-the-art CTMs.

3.1 Summary of model runs setup

C-IFS (CB05) was run from 1 January to 31 December 2008 with a spin up starting 1 July 2007 at a T255 resolution with 60 model levels in monthly chunks. The meteorological simulation was relaxed to dynamical fields of the MACC re-analysis (see section 2.1). Likewise stratospheric ozone above the tropopause was nudged to the MACC re-analysis.

MOZ is a run with the MOZART CTM at 1.1°×1.1° horizontal resolution using the 60 vertical levels of C-IFS. The meteorological fields used in MOZ were meteorological analyses provide by REAN. The setup of the MOZART model and the applied emissions and dry deposition velocities were the same in MOZ and REAN. The most important difference between MOZ and REAN is the assimilation of satellite retrieval of atmospheric composition in REAN. The assimilated retrievals were CO and ozone total columns, stratospheric ozone profiles and tropospheric NO_2 columns. No observations of atmospheric composition have been feed in to the MOZ run. No observational information has been used to improve the tropospheric simulation of the C-IFS run. Another difference between MOZ and REAN is that the IFS diffusion and convection scheme, as used in C-IFS, controls the vertical transport in REAN whereas MOZART's generic schemes were used in the MOZ run.

MOZ, REAN and C-IFS used the same anthropogenic emissions (MACCIty), biogenic emissions (MEGAN 2.1 Guenther et al., 2006, http://acd.ucar.edu/~guenther/MEGAN/MEGAN.htm) and natural emissions (POET). The biomass burning emissions for MOZ and REAN came from the GFED3 inventory which was redistributed according to the FRP observations used in GFAS. Hence, the average biomass burning emissions used by MOZART agree well with the GFAS emissions used by C-IFS, but they are not identical in the temporal and spatial variability.

3.2 Observations

The runs (C-IFS, MOZ, REAN) were evaluated with ozone observations from ozone sondes and ozone and CO aircraft profiles from the MOZAIC program. Simulated surface ozone, CO, NO_2 and SO_2 field were compared against GAW surface observations and additionally ozone against observations from the European air quality networks of the EMEP and AIRBASE data sets. The global distribution of tropospheric NO_2 and HCHO was evaluated with retrievals of tropospheric columns from GOME-2. MOPITT retrievals were used for the validation of the global CO total column fields.

3.2.1 In-situ observations

The ozone sondes were obtained from the World Ozone and Ultraviolet Radiation Data Centre (WOUDC) and from the ECWMF Meteorological Archive and Retrieval System. The observation error of the sondes is about ±5% in the range between 200 and 10 hPa and -7 - 17% below 200 hPa (Beekmann et al., 1994, Komhyr et al., 1995 and Steinbrecht et al., 1996). The number of soundings varied for the different stations. Typically, the sondes are launched once a week but in certain periods such as during ozone hole conditions soundings are more frequent. Ozone launches were carried out mostly between 9 and 12 hours local time. The global distribution of the launch sites is even enough to allow meaningful averages over larger areas such North-America, Europe, the Tropics, the Artic and Antarctica. *Table 2* contains a list of the ozone sondes used in this study.

The MOZAIC (Measurement of Ozone, Water Vapour, Carbon Monoxide and Nitrogen Oxides by Airbus in-service Aircraft) program (Marenco et al., 1998 and Nédélec et al., 2003) provides profiles of various trace gases taken during commercial aircraft ascents and descents at specific airports. MOZAIC CO data have an accuracy of ± 5 ppbv, a precision of ± 5%, and a detection limit of 10 ppbv (Nédélec et al., 2003). Since the aircraft carrying the MOZAIC unit were based in Frankfurt, the majority of the CO profiles (837 in 2008) were observed at this airport. Of the 28 airports with observations in 2008, only Windhoek (323), Caracas (129), Hyderabad (125) and London-Gatwick (83) as well as the North-American airports Atlanta (104), Portland (69), Philadelphia (65), Vancouver (56), Toronto (46) and Dallas (43) had a sufficient number of profiles. The North-American airports were considered to be close enough to make a spatial average meaningful.

Apart from Frankfurt, typically 2 profiles (start and landing) are taken within 2-3 hours or with a longer gap in the case of an overnight stay. At Frankfurt there were 2-6 profiles available each day, mostly in the morning and the later afternoon to the evening. At the other airports the typical observation times were 6 & 18 UTC for Windhoek (+/- 0 h local time), 19 & 21 UTC for Hyderabad (+ 4 h local time), 20 & 22 for Caracas (-6 h), 4 & 22 for London (+/- 0 h) and 19 & 22 (- 5/6 h) for the North American airports. This means that most of the observations were taken between the late evening and early morning hours, i.e. at a time of increased stability and large CO vertical gradients close to the surface. Only the observations at Caracas (afternoon) and to some extent in Frankfurt represent a more mixed day-time boundary layer.

The global atmospheric watch (GAW) program of the World Meteorological Organization is a network for mainly surface based observations (WMO, 2007). The data were retrieved from the World Data Centre for Greenhouse Gases [http://ds.data.jma.go.jp/gmd/wdcgg/]. The GAW observations represent the global background away from the main polluted areas. Often the GAW observation sites are located on mountains, which makes it necessary to select a model level different from the lowest model level for a sound comparison with the model. In this study the procedure described in

Flemming et al. (2009b) is applied to determine the model level, which is based on the difference between a high resolution orography and the actual station height. The data coverage for CO and ozone was global, whereas for SO_2 and NO_2 only a few observations in Europe were available at the data repository.

The Airbase and EMEP databases host operational air quality observations from different national European networks. All EMEP stations are located on rural areas, while Airbase stations are designed to monitor local pollution. Many AIRBASE observations may therefore not be representative for a global model with a horizontal resolution of 80 km. However, stations of rural regime may capture the larger scale signal in particular for ozone, which is spatially well correlated (Flemming et al., 2005). Only the rural Airbase ozone observations have been selected for the evaluation of the diurnal cycle.

Region	Area S/W/N/E	Stations (Number of observations)
Europe	35/-20/60/40	Barajas (52), DeBilt (57), Hohenpeissenberg (126), Legionowo (48), Lindenberg(52), Observatoire de Haute-Provence (46), Payerne (158), Prague (49), Uccle (142) and Valentia Observatory (49)
North America:	30/-135/60/-60	Boulder (65), Bratts Lake (61), Churchill (61), Egbert (29), Goose Bay (47), Kelowna (72), Stony Plain (77), Wallops (51), Yarmouth (60), Narragansett (7) and Trinidad Head (35)
Arctic:	60/-180/90/180	Alert (52), Eureka (83), Keflavik (8), Lerwick (49), Ny-Aalesund (77), Resolute (63), Scoresbysund (54), Sodankyla (63), Summit (81) and Thule(15)
Tropics	20/-180/20/180	Alajuela (47), Ascension Island (32), Hilo (47), Kuala Lumpur (24), Nairobi (39), Natal (48), Paramaribo (35), Poona (13), Samoa (33), San Cristobal (28), Suva (28), Thiruvananthapuram (12) and Watukosek (19)
East Asia	15/100/45/142	Hong Kong Observatory (49), Naha (37), Sapporo (42) and Tateno Tsukuba (49)
Antarctic	-90/-180/-60/180	Davis (24), Dumont d'Urville (38), Maitri (9), Marambio (66), Neumayer (72), South Pole (63), Syowa(41) and McMurdo (18)

Table 2 Ozone sondes sites used in the evaluation for different regions

3.2.2 Satellite retrievals

Satellite retrievals of atmospheric composition are more and more used to evaluate model results. Satellite data provide good horizontal coverage but have limitation with respect to the vertical resolution and signal from the lowest atmospheric levels. Further, satellite observations are only possible at the specific overpass time, and they can be disturbed by the presence of clouds and surface properties. Depending on the instrument type global coverage is achieved in several days.

Day-time CO total column retrievals, version 6 (Deeter et al., 2013b) from the Measurements Of Pollution In The Troposphere (MOPITT) instrument and retrievals of tropospheric columns of NO_2 (IUP-UB v0.7, Richter et al., 2005) and of HCHO (IUP-UB v1.0; Wittrock et al., 2006) from the Global Ozone Monitoring Exeriment-2 (GOME-2, Callies et al., 2000) have been used for the evaluation. The retrievals were spatially sampled, interpolated in time and finally averaged to monthly means values to further reduce the random retrieval error.

MOPITT is a multispectral thermal infrared (TIR) / near infrared (NIR) instrument onboard the TERRA satellite with a pixel resolution of 22 km. TERRA's local equatorial crossing time is approximately 10:30 a.m. The MOPITT CO pixels were binned within 1x1° within each month. Deeter et al. (2013a) report a bias of about +0.08e^{18} molec/cm^2 and a standard deviation (SD) of the error of 0.19e^{18} molec/cm^2 for product version 5. This is equivalent to a bias of about 4 % and a SD of 10% respectively assuming typical observations of 2.0 e^{18} molec/cm^2. For the calculation of the simulated CO total column the averaging kernels (AK) of the retrievals were applied. They have the largest values between 300 and 800 hPa. At surface the sensitivity is reduced even though the combined NIR/TIR product has been used, which has a higher sensitive than the NIR and TIR only products. Applying the AK makes the difference between retrieval and AK-weighted model column independent of the a-priori CO profiles used in the retrieval. On the other hand, it makes the total column calculation dependent on the modelled profile. The AK-weighted column is not equivalent to the modelled atmospheric burden anymore, which needs to be considered for the interpretation of the results.

GOME-2 is a UV-VIS and near-infrared sensor aboard the Meteorological Operational Satellite-A (MetOp-A) designed to provide global observations of atmospheric trace gases. Integrated tropospheric columns were retrieved at 9:30 local time. Uncertainties in NO_2 satellite retrievals are large and depend on the region and season. Winter values in mid and high latitudes are usually associated with larger error margins. As a rough estimate, systematic uncertainties in regions with significant pollution are of the order of 20% – 30%. As the HCHO retrieval is performed in the UV part of the spectrum where less light is available and the HCHO absorption signal is smaller than that of NO_2, the uncertainty of monthly mean HCHO columns is relatively large (20% – 40%) and both noise and systematic offsets have an influence on the results. However, absolute values and seasonality are retrieved more accurately over HCHO hotspots.

3.3 Tropospheric Ozone

Figure 2 shows the monthly means of ozone volume mixing ratios in the pressure ranges surface to 700 hPa (lower troposphere, LT) 700-400 hPa (middle troposphere, MT) and 400-200 hPa (upper troposphere UT) observed by sondes and averaged over Europe, North America and East Asia. Figure 3 shows the same as Figure 2 for the Tropics, Artic and Antarctica. The observations have a pronounced spring maximum for UT ozone over Europe, North America and East Asia and a more gradually developing maximum in late spring and summer in MT and LT. The LT seasonal cycle is well re-produced in all runs for the areas of the Northern Hemisphere (NH). In Europe, REAN tends to overestimate by about 5 ppb where the C-IFS and MOZ have almost no bias before the annual maximum in May apart from a small negative bias in spring. Later in the year, C-IFS tends to overestimate in autumn, whereas MOZ overestimates more in late summer. In MT over Europe C-IFS agrees slightly better with the observations than MOZ. MOZ overestimates in winter and spring and this overestimation is more prominent in the UT, where MOZ is biased high throughout the year. This overestimation in UT is highest in spring, where it can be 25% and more. These findings show that data assimilation in REAN improved UT ozone considerably but had only little influence in LT and MT. The overestimation of MOZ in UT seems to be caused by increased stratospheric ozone rather than a more efficient transport. The good agreement of C-IFS with observation in UT in all three regions is also present in a run without nudging to stratospheric ozone. It is therefore not a consequence of the use of assimilated observations in C-IFS (CB05).

Over North-America the spring time underestimation by C-IFS and MOZ is more pronounced than over Europe. C-IFS also underestimated MT ozone observations in this period, whereas MOZ and REAN slightly overestimate. In East Asia all runs overestimate by 5-10 ppb in LT and MT especially in autumn and winter. In the northern high latitudes (Figure 3) the negative spring bias appears in all runs in LT and only for C-IFS in MT. As in the other regions, MOZ greatly overestimates UT ozone.

Averaged over the tropics, the annual variability is below 10 ppb with maxima in May in September caused by the dry season in South-America (May) and Africa (September). The variability is well reproduced and biases are mostly below 5 ppb in the whole troposphere. Note that the 400-200 hPa range (UT) in the tropics is less influenced by the stratosphere because of the higher tropopause. C-IFS had smaller biases because of lower values in LT and higher values in MT and UT than MOZ.

Over the Arctic C-IFS and MOZ reproduce the seasonal cycle, which peaks in late spring, but generally underestimate the observations in LT. C-IFS had a smaller bias in LT than MOZ but had a larger negative bias in MT. The biggest improvement of C-IFS w.r.t to MOZ occurred at the surface in Antarctica as the biases compared to the GAW surface observations were greatly reduced. Notably, the assimilation (REAN) led to increased biases for LT and MT ozone, in particular during polar night when UV satellite observations are not available as already discussed in Flemming et al. (2011a).

The ability of the models to simulate ozone near the surface is tested with rural AIRBASE and EMEP stations in Europe (see section 3.2). Figure 4 shows monthly means and Figure 5 the average diurnal cycle in different season. All runs underestimate monthly mean ozone in spring and winter and overestimate it in late summer and autumn. The overestimation in summer was largest in MOZ. While the overestimation appeared also with respect to the ozone sondes in LT (see Figure 2, left) the spring time underestimation was less pronounced in LT.

The comparison of the diurnal cycle with observations (Figure 5) shows that C-IFS produced a more realistic diurnal cycle than the MOZART model. The diurnal variability simulated by the MOZART model is much less pronounced than the observations suggest. The diurnal cycle of C-IFS and REAN were similar. This finding can be explained by the fact that C-IFS and REAN use the IFS diffusion scheme whereas MOZART applies the diffusion scheme of the MOZART CTM.

The negative bias of C-IFS in winter and spring seems mainly caused by an underestimation of the night time values whereas the overestimation of the summer and autumn average values in C-IFS were caused by an overestimation of the day time values. However, the overestimation of the summer night time values by MOZART seems to be a strong contribution to the average overestimation in this season.

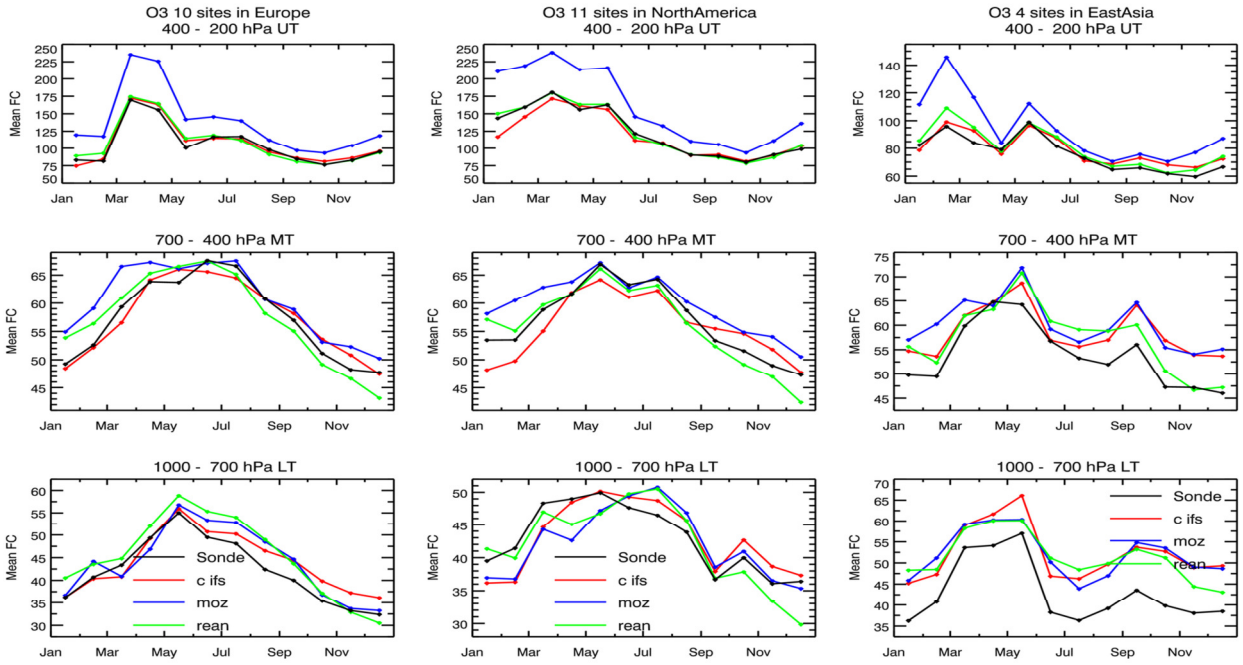

Figure 2 Tropospheric ozone volume mixing ratios (ppb) over Europe (left) and North-America (middle) and East Asia (right) averaged in the pressure range 1000-700 hPa (bottom), 700-400 hPa (middle) and 400-200 hPa (top) observed by ozones sonde (black) and simulated by C-IFS (red), MOZ (blue) and REAN (green) in 2008.

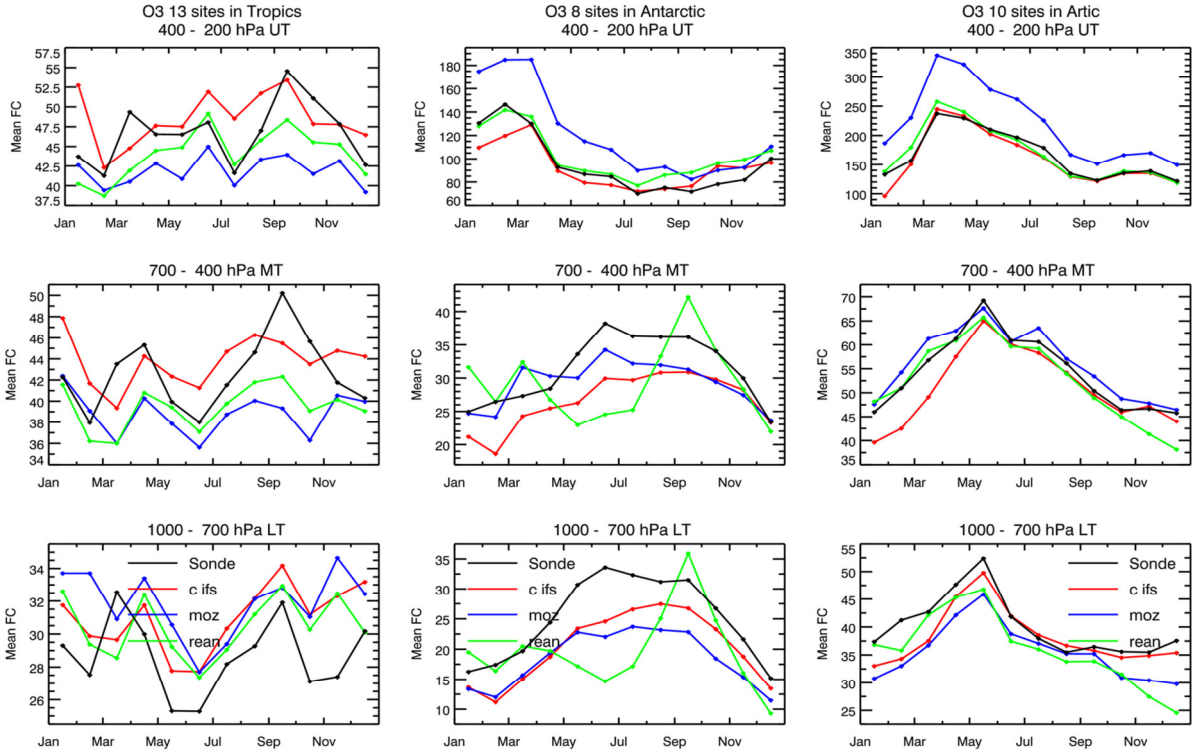

Figure 3 Tropospheric ozone volume mixing ratios (ppb) over the Tropics (left) Arctic (middle) and Antarctica (right) averaged in the pressure bands 1000-700 hPa (bottom), 700-400 hPa (middle) and 400-200 hPa (top) observed by ozone sondes and simulated by C-IFS (red), MOZ (blue) and REAN (green) in 2008.

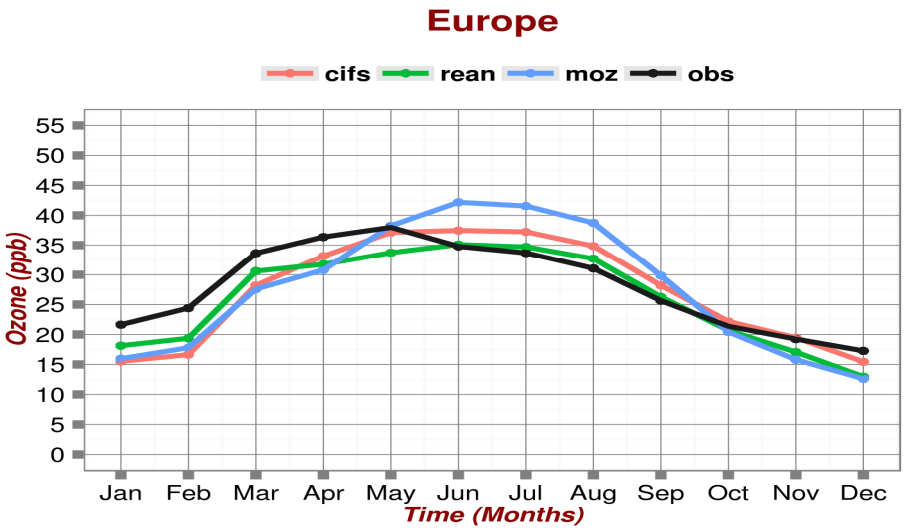

Figure 4 Annual cycle of the mean ozone volume mixing ratios (ppb) at rural sites of the EMEP and AIRBASE data base and simulated by C-IFS and MOZ and REAN.

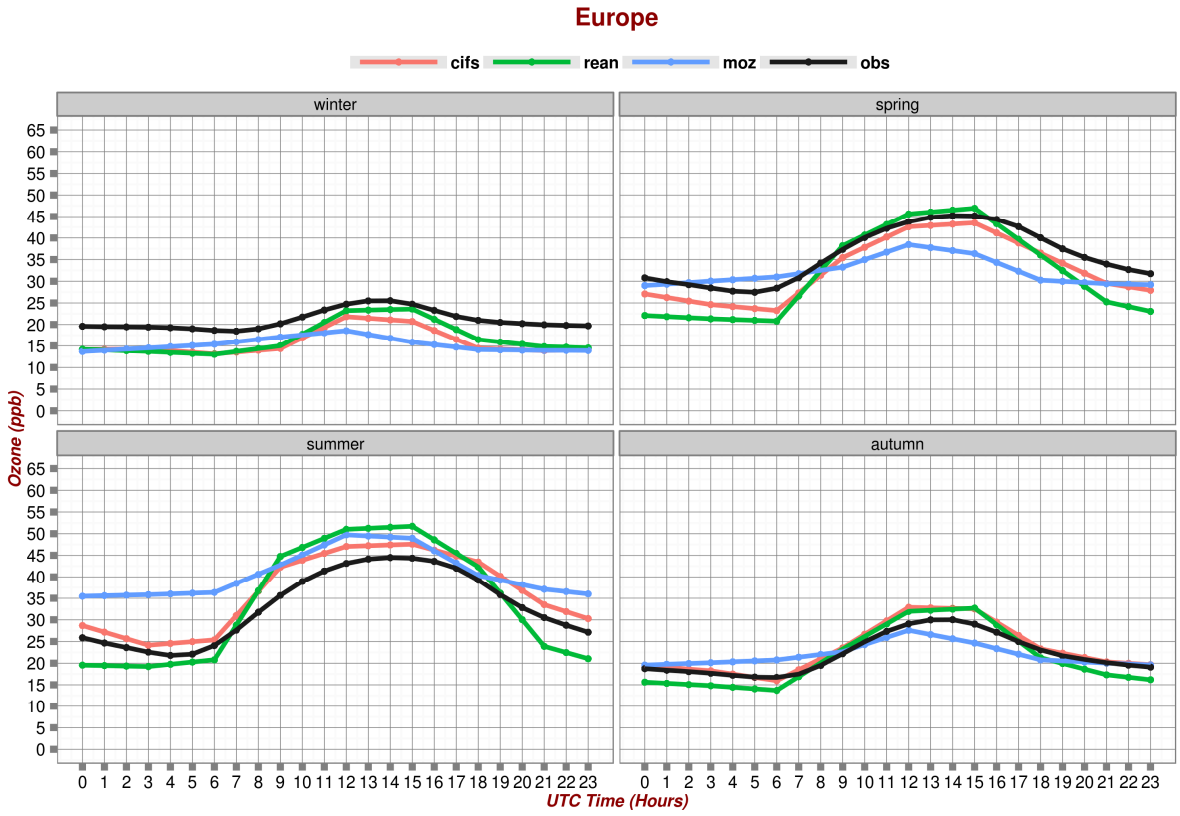

Figure 5 Diurnal cycle of surface ozone volume mixing ratios (ppb) over Europe in different seasons at rural site of the EMEP and AIRBASE data base and simulated by C-IFS and MOZ and REAN.

3.4 Carbon Monoxide

The seasonality of CO is mainly driven by its chemical lifetime, which is lower in summer because of increased photochemical activity. The seasonal variability of the CO emissions plays also an important role in particular in the case of biomass burning. The global distribution of total column CO retrieved from MOPITT and from AK weighted columns simulated by C-IFS, MOZ and REAN is shown for April 2008 in Figure 6 and for August in Figure 7. April and August have been selected because they are the months of the NH CO maximum and minimum. C-IFS reproduced well the observed global maxima in North-America, Europe and China as well as the biomass burning signal in Central Africa. However, there was a widespread underestimation of the MOPITT values in the NH, which was strongest over European Russia and Northern China. Tropical CO was slightly overestimated but more strongly over Southeast Asia in April at the end of the biomass burning season in this region. The lower CO columns in mid- and high latitudes in the Southern Hemisphere (SH) were underestimated. The same global gradients of the bias were found in MOZ and REAN. The negative NH bias in April of MOZ is however more pronounced but the positive bias in the tropics is slightly reduced. The bias of MOZ seems stronger over the entire land surface in NH and not predominately in the areas with high emission. This is consistent with the finding of Stein et al. (2014) that dry deposition, besides underestimated emissions, contributes to the large negative biases in NH in MOZ. Assimilating MOPITT (V4) in REAN led to much reduced biases everywhere even though the sign of bias in NH, Tropics and SH remained. In August, the NH bias is reduced but the hemispheric pattern of the CO bias was similar as in April for all runs. The only regional exception from the general overestimation in the tropics is the strong underestimation of CO in the biomass burning maximum in Southern Africa, which points to an underestimation of the GFAS biomass burning emissions in that area.

More insight in the seasonal cycle and the vertical CO distribution can be obtained from MOZAIC air craft profiles. CO profiles at Frankfurt (Figure 8, left) provide a continuous record with about 2 - 6 observations per day. As already reported in Inness et al. (2013) and Stein et al. (2014), MOZ underestimates strongly LT CO with a negative bias of 40 - 60 ppb throughout the whole year. The highest underestimation occurred in April and May, i.e. at the time of the observed CO maximum. C-IFS CB05 also underestimates CO but with a smaller negative bias in the range of 20-40 ppb even though it used the same CO emission data as MOZ. REAN has the lowest bias throughout the year but the improvement is more important in winter and early spring. The comparison over London, which is representative for 4 and 22 UTC, leads to similar results as for Frankfurt (Figure 8, middle). The outcome of the comparison with LT CO from MOZAIC is consistent with the model bias with respect to the GAW surface observations in Europe in Figure 10. The seasonal variability of LT CO from MOZAIC and the model runs in North-America is very similar to the one in Europe (Figure 8, right). The late winter and spring bias is slightly increased whereas the summer time bias was lower for all models. The surface bias in winter and spring of MOZ, C-IFS and REAN is about -50, -40 and -20 ppb respectively. In the rest of the year REAN and C-IFS have a bias of about -15 ppb whereas the bias of MOZ is about twice as large.

MT CO was very well produced by REAN in Europe and North-America probably because MOPITT has the highest sensitivity at this level. The MT bias of C-IFS is about 75% of the bias of MOZ, which underestimates by about 30 ppb. In the UT the CO biases are for all models mostly below 10ppb, i.e. about 10 %. C-IFS has overall the smallest CO bias whereas REAN tends to overestimate and MOZ to underestimate CO over Europe and North America.

CO observed by MOZAIC over Windhoek (Figure 9, middle) has a pronounced maximum in September because of the seasonality of biomass burning in this region. Although all runs show increased CO in this period, the models without assimilation were less able to reproduce the high observed CO values and are biased low up to 40 ppb in LT and MT. Biases were much reduced, i.e. mostly within 10 ppb, during the rest of the year. The assimilation in REAN greatly reduces the bias in the biomass burning period. In UT C-IFS had slightly smaller biases of about 10 ppb than MOZ and REAN. A less complete record of the seasonal variability is available for Caracas (Figure 9, left). All models tend to underestimate UT and MT CO maxima in April by about 20% but in contrast to Windhoek the C-IFS and not REAN has the smallest bias in LT. Hyderabad (Figure 9, right) is the only observation site were a substantial overestimation of CO in LT and UT is present even though the observations are in the range of 150 - 250 ppb, which is mostly higher than at any of the other airports discussed. All models overestimate the seasonality because of an underestimation in JJA and an overestimation during the rest of the year.

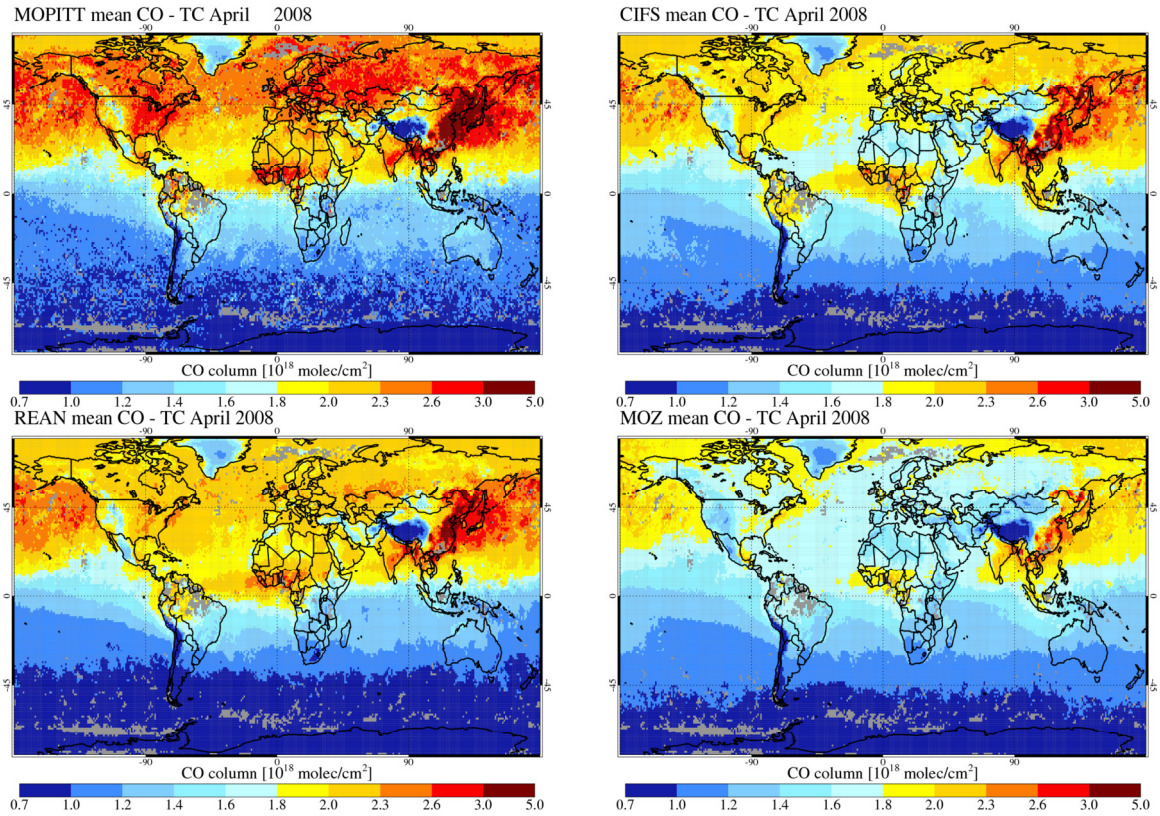

Figure 6 CO total column retrieval (MOPITT V6) for April 2008 (top left) and simulated by C-IFS (top right), MOZ (bottom left) and REAN (bottom right), AK are applied.

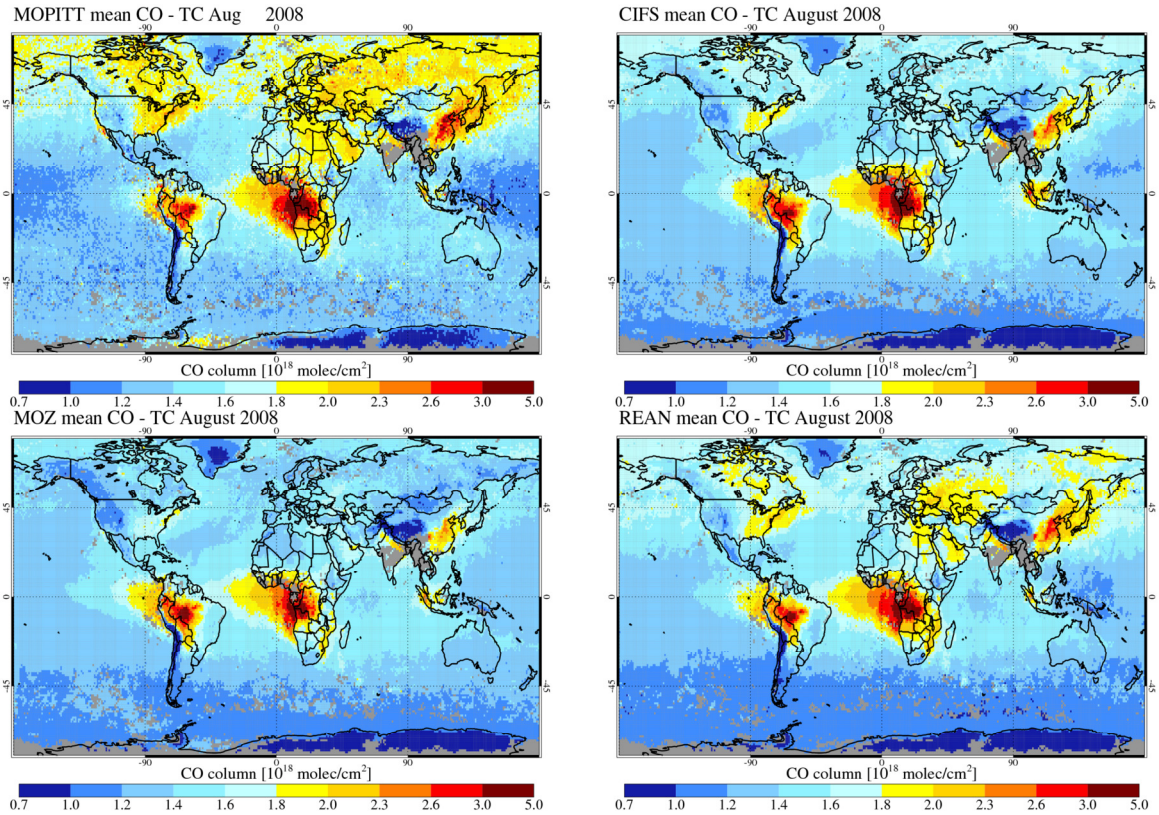

Figure 7 CO total column retrieval (MOPITT V6) for August 2008 (top left) and simulated by C-IFS (top right), MOZ (bottom right) and REAN (bottom left), AK are applied.

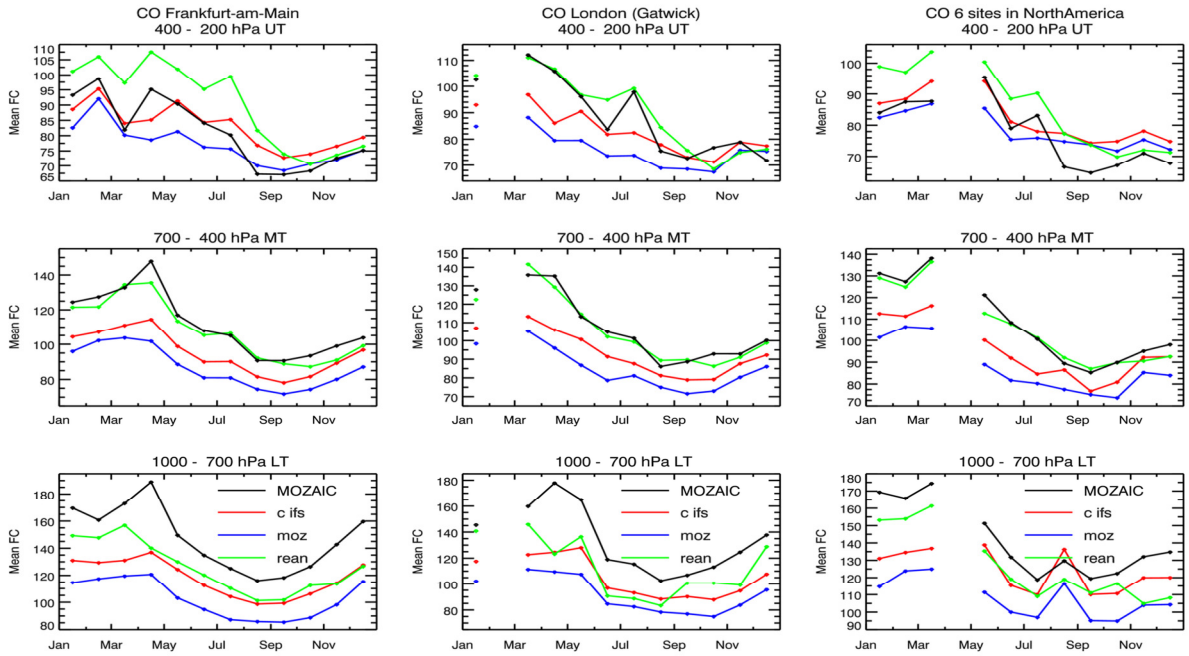

Figure 8 CO volume mixing ratios (ppb) over Frankfurt (left), London (middle) and North America (left, averaged over 8 airports) averaged in the pressure bands 1000-700 hPa (bottom), 700-400 hPa (middle) and 400-200 hPa (top) observed by MOZAIC and simulated by C-IFS (red), MOZ (blue) and REAN (green) in 2008.

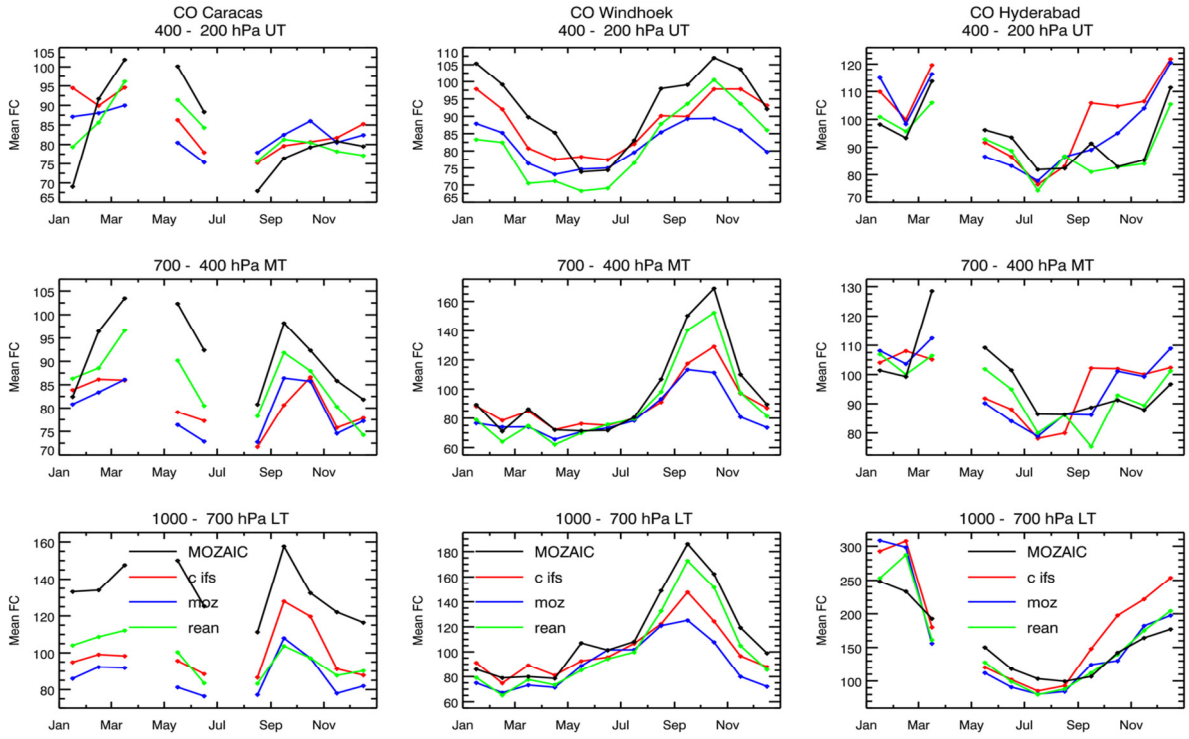

Figure 9 CO volume mixing ratios (ppb) over Caracas (left) Windhoek (middle) and Hyderabad (right) averaged in the pressure bands 1000-700 hPa (bottom), 700-400 hPa (middle) and 400-200 hPa (top) observed by MOZAIC, and simulated by C-IFS (red), MOZ (blue) and REAN (green) in 2008.

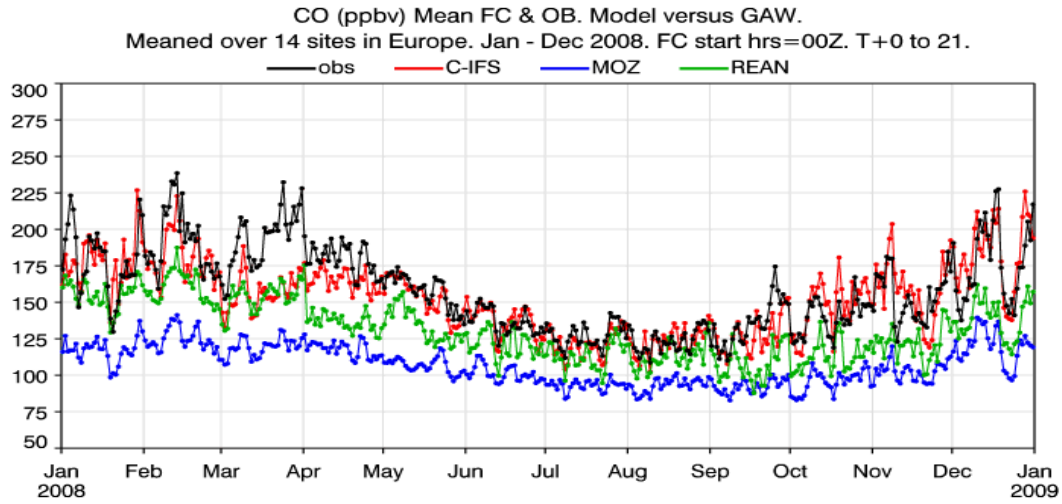

Figure 10 Time series of CO volume mixing ratios (ppb) in Europe at the surface averaged over 14 GAW sites and from C-IFS, MOZ and REAN.

3.5 Nitrogen dioxide

The global maxima of NO_2 are located in areas of high anthropogenic and biomass burning NO emissions. The global annual distribution of annual tropospheric columns retrieved from the GOME-2 instrument and simulated by the models is shown in Figure 11. C-IFS, MOZ and REAN showed a very similar distribution, which can be explained by that fact that the same NO emission data were used in all runs. The global patterns of the modelled fields resemble the observed annual patterns to a large extent. But the models tend to underestimate the high observed values in East-Asia and Europe and also simulate too little NO_2 in larger areas of medium observed NO_2 levels in Asia and Central Africa as well as in the outflow areas over the West-Atlantic and West Pacific Ocean. This could mean that NO emissions in the most polluted areas are too low but also that the simulated lifetime of NO_2 is too short.

The validation of the seasonality of NO_2 (Figure 12) for different regions and months shows that tropospheric NO_2 columns over Europe North America, South Africa and East-Asia are reasonably reproduced. The models tend to underestimate tropospheric columns over Europe in summer. However, the evaluation with GAW surface stations (Figure 13) shows a positive bias for REAN throughout the year but particularly in winter. C-IFS had a moderate positive bias at the surface in summer whereas MOZ has nearly no bias in this season. All runs significantly underestimate the annual cycle of the GOME-2 NO_2 columns over East-Asia. The winter time values are only half of the observations whereas in summer models agree well with observations. In Southern Africa, the models overestimate the increased NO_2 values in the biomass burning season by a factor 2 but show good agreement with observations in the rest of the year.

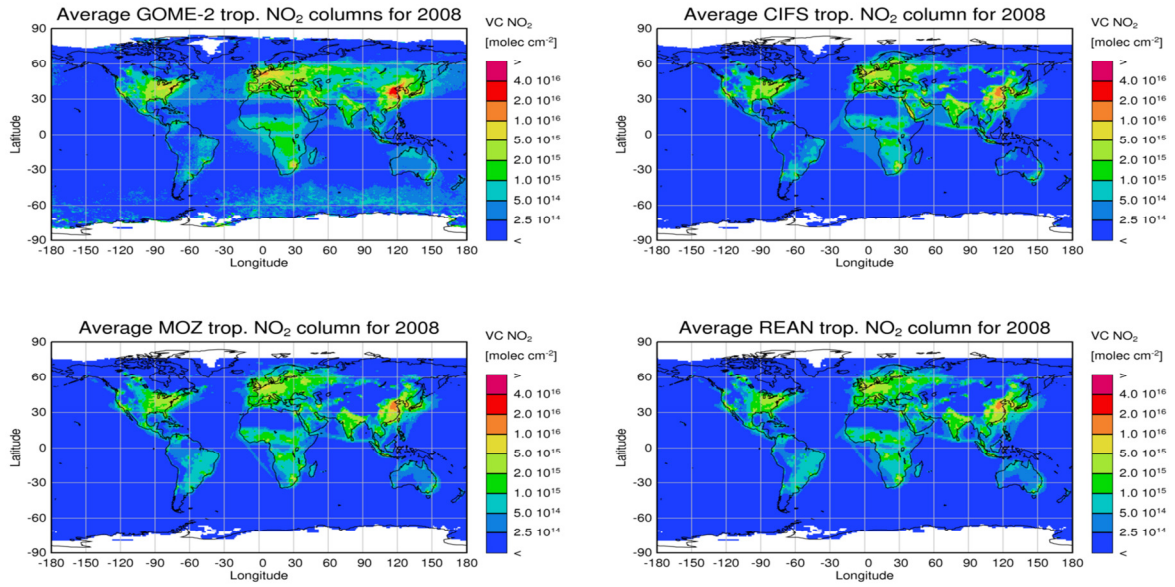

Figure 11 NO_2 tropospheric column retrieval (GOME-2) for 2008 (top left) and by C-IFS (top right), REAN (bottom right) and MOZ (bottom left)

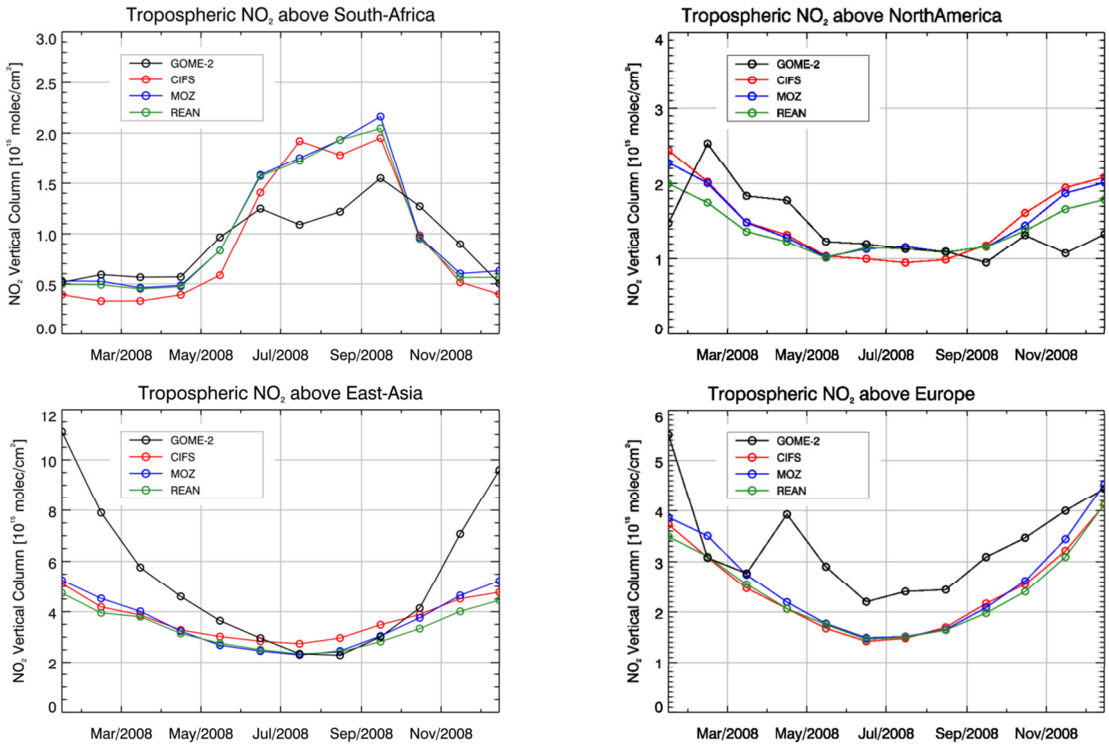

Figure 12 Time series of area-averaged tropospheric NO_2 columns [10^{15} molec cm-2] from GOME-2 compared to model results for C-IFS (CB05) (blue), MOZ (red) and REAN (green) for different regions.

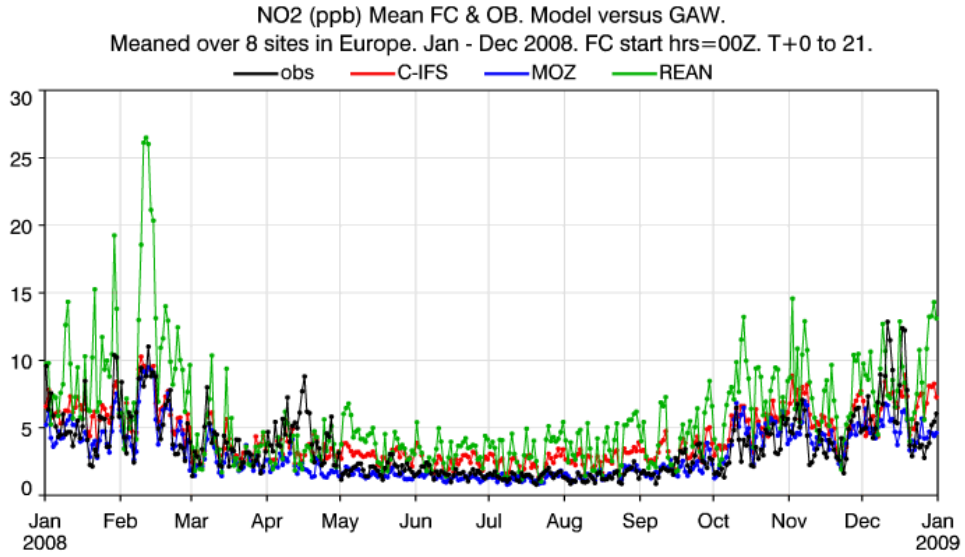

Figure 13 Time series of NO_2 volume mixing ratios (ppb) in Europe at the surface averaged over 8 GAW sites and from C-IFS, MOZ and REAN

3.6 Formaldehyde

On the global scale Formaldehyde (HCHO) is mainly chemically produced by the oxidation of isoprene and methane. Isoprene is emitted by vegetation. On the regional scale HCHO emissions from anthropogenic sources, vegetation and biomass burning also contribute to the HCHO burden.

The annual average of tropospheric HCHO retrieved from GOME-2 and from the model runs is shown in Figure 14. The observations show higher values in the tropics and the NH and maxima in the rain forest regions of South America and Central Africa and in South East Asia. The simulated fields of the three runs are very similar. C-IFS, MOZ and REAN reproduce the observed global patterns but show a small but widespread underestimation in the NH extra-Tropics and in industrialized East Asia. On the other hand HCHO is overestimated in Indonesia.

Figure 15 shows model time series of tropospheric HCHO against corresponding GOME-2 satellite retrievals for selected regions. The models underestimated satellite values over East-Asia especially in summer and overestimate HCHO columns for Indonesia throughout the year. The seasonality in Southern Africa (not shown) and South America is well captured in particular by C-IFS. All models also reproduced the observations rather well for the Eastern United States, but tend to underestimate wintertime HCHO columns for this region.

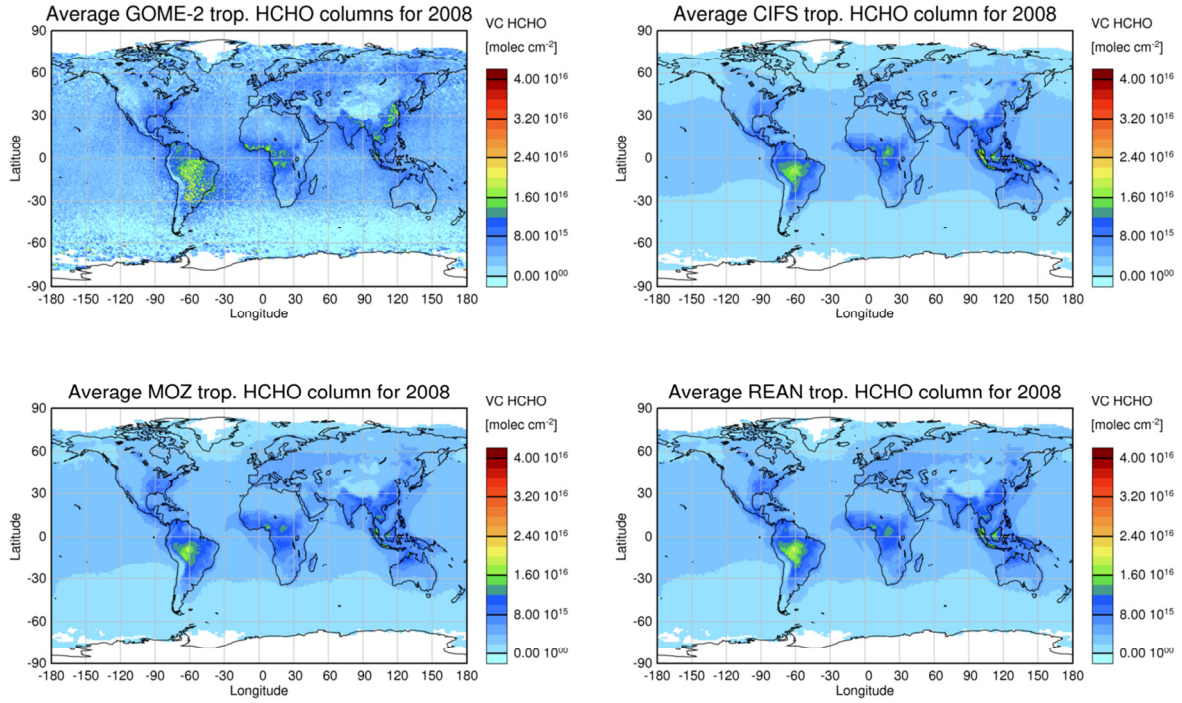

Figure 14 HCHO tropospheric column retrieval (GOME-2) for 2008 (top left) and by C-IFS (top right), REAN (bottom right) and MOZ (bottom left)

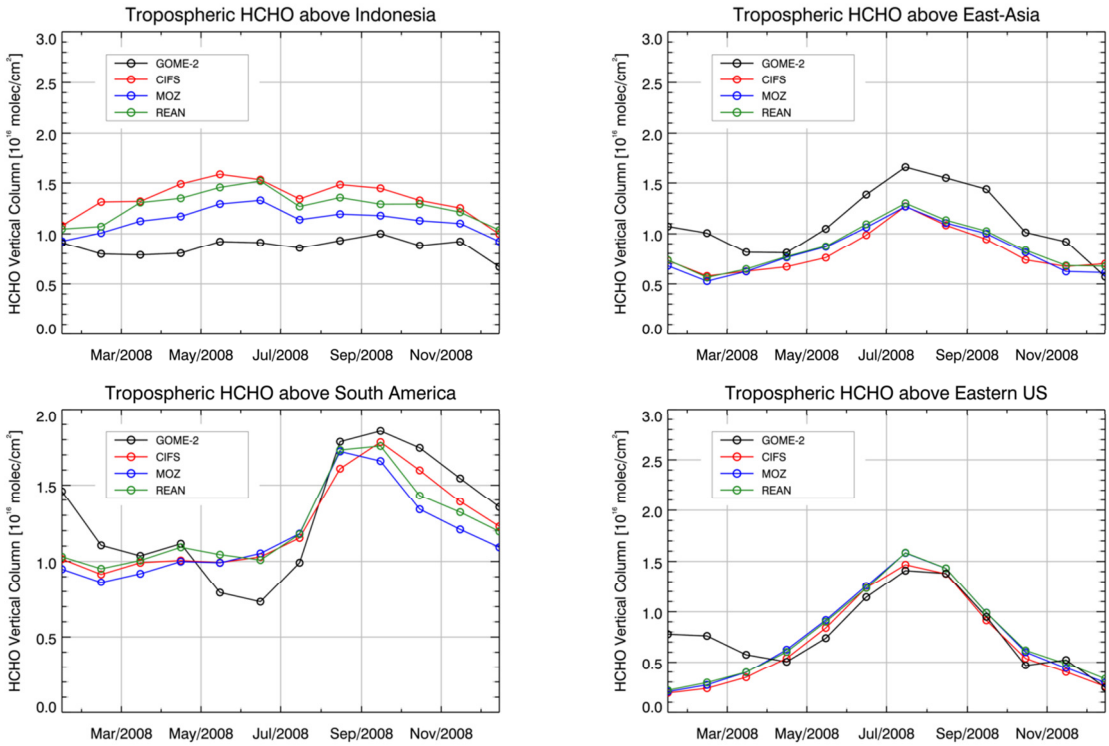

Figure 15 Time series of area-averaged tropospheric HCHO columns [10^{16} molec cm-2] from GOME-2 compared to model results for C-IFS, MOZ and REAN for different regions.

3.7 Sulfur dioxide

SO_2 was evaluated in Europe using GAW surface observations. Figure 16 shows a time series of the averaged daily values. All models suffer from a positive winter time bias, which is largest for REAN and smallest for C-IFS. As no SO_2 observations were assimilated in REAN and identical SO_2 emission were used, the differences between the runs were caused by differences in the simulation of vertical mixing, sulfur chemistry and wet and dry deposition in C-IFS and MOZART. As for NO_2, the largest bias was simulated by the coupled system, i.e. REAN. It could be caused by inconsistencies in the coupled approach in particular at the surface: In the coupled approach, dry deposition loss terms were calculated in MOZART based on the concentrations values at surface. The loss terms were then applied to the IFS concentration without accounting for the different tracer distribution in IFS because of different diffusion schemes in MOZART and IFS. Overall, the on-line integration of C-IFS shows the lowest SO_2 biases. As already pointed out for the comparison with AIRBASE surface ozone data, C-IFS simulated the most realistic diurnal variability.

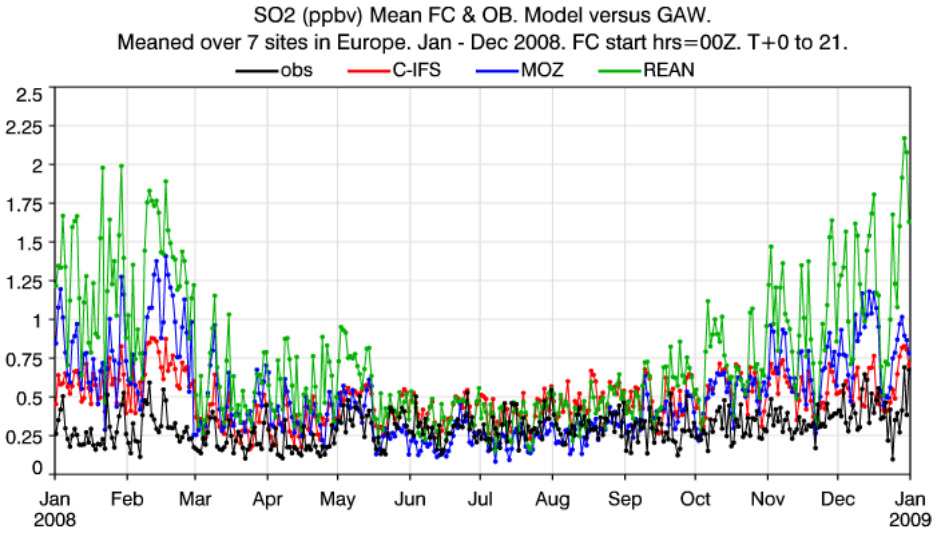

Figure 16 Time series of SO_2 volume mixing ratios (ppb) in Europe at the surface averaged over 7 GAW sites and from C-IFS, MOZ and REAN

3.8 Computational cost

The computational cost is an important factor for the operational applications in CAMS. The computational cost of different configurations of IFS, C-IFS and IFS-MOZART are given in Table 3. Computational cost is expressed in billing units (BU) of the ECMWF IBM Power 7 super-computer. BUs are proportional to the number of used CPU times the simulation time.

The increase of cost because of the simulation of the CB05 chemistry with respect to an NWP run is about a factor 4 at the resolution T159 (110km), T255 (80 km) and T511 (40 km). C-IFS (CB05) is about 8 times more efficient than the coupled system IFS-MOZART at a T159 resolution and about 15 times more at a T255 resolution. This strong relative increase in cost of IFS-MOZART is caused by the increasing memory requirements of the IFS at higher resolution, or also in data assimilation mode. The additional resources allocated to the IFS are however mostly latent as the coupled MOZART model can not be made faster by using more resources.

C-IFS with the MOZART chemical mechanism, i.e. the same chemistry scheme as in IFS-MOZART, is about 2 times and C-IFS with RACMOBUS 7 times more costly than C-IFS (CB05) at a T159 resolution. Both the MOZART and the RACMOBUS scheme encompass a larger number of species and reactions and include a full stratospheric chemistry scheme, which is missing in CB05.

	IFS-MOZART	C-IFS (MOZART)*	C-IFS (MOCAGE)*	C-IFS (CB05)	IFS
T159	205	56	147	20	6
T255	1200	-	-	55	12
T511	-	-	-	700	125

*Table 3 Computational cost (BU) of a 24 h forecasts of different horizontal model resolutions (60 levels) and chemistry schemes of C-IFS, IFS-MOZART and IFS, *not fully optimised.*

4 Summary and outlook

Modules for the simulation of atmospheric chemistry have been implemented on-line in the Integrated Forecasting System (IFS) of ECMWF. The chemistry scheme complements the already integrated modules for aerosol and greenhouse gases as part of the IFS for atmospheric Composition (C-IFS). C-IFS for chemistry replaces the coupled system IFS-MOZART for forecast and assimilation of reactive gases within the pre-operational Copernicus Atmosphere Monitoring Service.

C-IFS applies the chemical mechanism CB05, which describes tropospheric chemistry with 55 species and 126 reactions. C-IFS benefits from the detailed cloud and precipitation physics of the IFS for the calculation of wet deposition and lightning NO emission. Wet deposition modelling is based on Jacob (2000) and accounts for the sub-grid scale distribution of clouds and precipitation. Dry deposition is modelled using pre-calculated monthly-mean dry deposition velocities following (Wesely, 1989) with a superimposed diurnal cycle. Lightning emissions of NO can be calculated either by cloud height (Price and Rind, 1993) or by convective precipitation (Meijer et al., 2010). The latter parameterization was used in this study. The anthropogenic emissions were taken from the MACCity inventory and biomass burning emissions from the GFAS data set for 2008.

An evaluation for the troposphere of a simulation in 2008 with C-IFS CB05 and the MOZART CTM (MOZ) as well as with the MACC re-analysis (REAN) was carried out. The model results were compared against ozone sondes, MOZAIC CO aircraft profiles, European surface observations of ozone, CO, SO_2 and NO_2 and global satellite retrievals of CO, NO_2 and HCHO. The evaluation showed that C-IFS preforms better or with similar accuracy as MOZART and mostly of similar quality as the MACC re-analysis. It should be noted that satellite retrievals of CO, ozone and NO_2 were assimilated in the MACC re-analysis to improve the realism of the fields simulated by IFS-MOZART.

In comparison to MOZ, C-IFS CB05 had smaller biases (i) for CO in the Northern Hemisphere, (ii) for ozone in the upper troposphere and (ii) for winter-time SO_2 at the surface in Europe. Further, the diurnal cycle of surface ozone, tested with rural European Air quality observations, showed greater realism in the C-IFS simulation. As both models used the same emission data, the improvements can be explained by the differences in the chemical mechanism and the simulation of wet and dry deposition. However, the improvements in SO_2 and the diurnal cycle of ozone are most probably caused by the more consistent interplay of diffusion and sink and sources processes in the on-line integrated C-IFS.

There is still room for improvement of C-IFS (CB05). It underestimated surface ozone over Europe and North America in spring and overestimated it in late summer and autumn. CO was still underestimated by C-IFS in particular in Europe and North America throughout the year but more in spring and winter, and in the biomass burning season in Africa. Winter time tropospheric NO_2 over China as retrieved from the GOME-2 instrument was two times higher than the fields modelled by C-IFS, MOZART and the MACC re-analysis.

Although only one chemical mechanism is described in the paper, C-IFS is a model that can apply multiple chemistry schemes. The implementation of the chemistry schemes of the CTMs MOCAGE and MOZART has technically been completed but further optimisation and evaluation is required. Both schemes offer a description of stratospheric chemistry, which is not included in the tropospheric scheme CB05. For this reason it is intended to combine the CB05 mechanism with the BASCOE

stratospheric mechanism. An inter-comparison of the performance of the different chemical mechanism is planned.

It is foreseen to further improve the link between the physics and chemistry packages in IFS. For example, the detailed information from the IFS surface scheme will be utilised for the calculation of dry deposition and biogenic emissions. A first important step is to replace the climatological dry deposition velocities with-online calculated timely values. Further, the impact of the simulated ozone fields, once the stratospheric chemistry is fully implemented, on the IFS radiation scheme and the corresponding feedback on the temperature fields will be investigated.

Another ongoing development direction is to link more closely the aerosol and gas-phase chemistry modules of C-IFS. Relevant chemical conversion terms can already be fed to the GLOMAP aerosol (Mann et al, 2010) module for the simulation of secondary aerosols. The calculation of photolysis rates can account for the presence of aerosols and HO_2 uptake on aerosols can be simulated (Huijnen, Williams and Flemming, 2014).

In summary, C-IFS is a new global chemistry weather model for forecast and assimilation of atmospheric composition. C-IFS (CB05) has already been successfully applied in data assimilation mode and a paper on the subject is in preparation (Inness et al., 2014). C-IFS offers improvements over the coupled system IFS-MOZART because (i) it simulates several trace gases with better accuracy, (ii) it is computational several times more efficient in particular at high resolution and (iii) it better facilitates the implementation of feedback processes between gas-phase and aerosol processes as well as between atmospheric composition and meteorology.

Acknowledgments

MACC II is funded by the European Union's Seventh Framework Programme (FP7) under Grant Agreement no. 283576. The MOPITT data were obtained from the NASA Langley Research Atmospheric Science Data Center. We are grateful to the World Ozone and Ultraviolet Radiation Data Centre (WOUDC) for providing ozone sonde obervations. We thank the Global Atmospheric Watch programme for the provision of NO_2, CO and SO_2 surface observations. We thank the European Environmental Agency for providing access to European ozone observations in the AirBase data base. We also thank the MOZAIC (Measurements of OZone, water vapour, carbon monoxide and nitrogen oxides by in-service AIrbus aircraft) and IAGOS (In-Service Aircraft for a Global Observing System) programmes for providing CO profile observations.

References

Archibald, A.T., Jenkin, M.E., Shallcross, D.E: An isoprene mechanism intercomparison, Atmospheric Environment, Volume 44, Issue 40, 2010, pp 5356-5364, http://dx.doi.org/10.1016/j.atmosenv.2009.09.016., 2009.

Atkinson, R., Baulch, D. L., Cox, R. A., Crowley, J, N., Hampson, R. F., Hynes, R. G., Jenkin, M. E., Rossi, M. J. and Troe, J.: evaluated kinetic and photochemical data for atmospheric chemistry: Volume I – gas phase reactions of Ox, HOx, NOx and SOx, species, Atmos. Chem. Phys., 4, 1461–1738, doi:10.5194/acp-4-1461-2004, 2004.

Atkinson, R., Baulch, D. L., Cox, R. A., Crowley, J. N., Hampson, R. F., Hynes, R. G., Jenkin, M. E., Rossi, M. J., Troe, J., and IUPAC Subcommittee: Evaluated kinetic and photochemical data for atmospheric chemistry: Volume II – gas phase reactions of organic species, Atmos. Chem. Phys., 6, 3625–4055, doi:10.5194/acp-6-3625-2006, 2006.

Baklanov, A., Schlünzen, K., Suppan, P., Baldasano, J., Brunner, D., Aksoyoglu, S., Carmichael, G., Douros, J., Flemming, J., Forkel, R., Galmarini, S., Gauss, M., Grell, G., Hirtl, M., Joffre, S., Jorba, O., Kaas, E., Kaasik, M., Kallos, G., Kong, X., Korsholm, U., Kurganskiy, A., Kushta, J., Lohmann, U., Mahura, A., Manders-Groot, A., Maurizi, A., Moussiopoulos, N., Rao, S. T., Savage, N., Seigneur, C., Sokhi, R. S., Solazzo, E., Solomos, S., Sørensen, B., Tsegas, G., Vignati, E., Vogel, B., and Zhang, Y.: Online coupled regional meteorology chemistry models in Europe: current status and prospects, Atmos. Chem. Phys., 14, 317-398, doi:10.5194/acp-14-317-2014, 2014.

Barkley, M., Description of MEGAN biogenic VOC emissions in GEOS-Chem, 2010. http://acmg.seas.harvard.edu/geos/wiki_docs/emissions/megan.pdf

Bechtold, P., Semane, N., Lopez, P., Chaboureau, J-P, Beljaars, A., Bormann, N: 2014: Representing Equilibrium and Nonequilibrium Convection in Large-Scale Models. J. Atmos. Sci., 71, 734–753. doi: http://dx.doi.org/10.1175/JAS-D-13-0163.1. 2014

Beekmann M., Ancellet G., Megie G., Smit H. G. J., and Kley D.: Intercomparison campaign for vertical ozone profiles including electrochemical sondes of ECC and Brewer-Mast type and aground based UV-differential absorption radar, J. Atmos. Chem., 10, 259–288, 1994

Beljaars, A.C.M. and P. Viterbo,: The role of the boundary layer in a numerical weather prediction model, in: Clear and cloudy boundary layers, A.A.M. Holtslag and P. Duynkerke (eds.), Royal Netherlands Academy of Arts and Sciences, p. 287-304, Amsterdam, North Holland Publishers, 1998.

Beljaars, A., Bechtold, P., Kohler, M., Morcrette, J-J., Tompkins, A., Viterbo, P. and Wedi, N.: The numerics of physical parameterization, Seminar on Recent developments in numerical methods for atmospheric and ocean modelling, 6-10 September, http://www.ecmwf.int/publications/library/do/references/, 2004.

Benedetti, A., Morcrette, J.-J., Boucher, O., Dethof, A., Engelen, R. J., Fisher, M., Flentje, H., Huneeus, N., Jones, L.,Kaiser, J. W., Kinne, S., Mangold, A., Razinger, M.,Simmons, A. J., Suttie, M., and the GEMS-AER team: Aerosol analysis and forecast in the European Centre for Medium-Range Weather Forecasts Integrated Forecast System: 2. Data assimilation, J. Geophys. Res., 114, D13205, doi:10.1029/2008JD011115, 2009.

Bousserez, N., Attié, J.-L., Peuch, V.-H., Michou, M., and Pfister, G.: Evaluation of the MOCAGE chemistry and transport model during the ICARTT/ITOP experiment, J. Geophys. Res., 112, D10S42, doi:10.1029/2006JD007595, 2007.

Callies, J., Corpacicioli, E., Eisinger, M., Hahne, A., and Lefebvre, A.: GOME-2 Metops's Second Generation Sensor for Operational Ozone Monitoring, ESA Bulletin, 102, 2000.

Cariolle, D. and Deque, M.:. Southern hemisphere medium-scale waves and total ozone disturbances in a spectral general circulation model, J. Geophys. Res., 91D, 10825–10846, 1986.

Cariolle, D. and Teyssèdre, H.: A revised linear ozone photochemistry parameterization for use in transport and general circulation models: multi-annual simulations, Atmos. Chem. Phys., 7, 2183-2196, doi:10.5194/acp-7-2183-2007, 2007.

Carslaw, K. S., Luo, B., Peter, T., and Clegg, S. L.: Vapour pressures of H2SO4/HNO3/HBr/H2O solutions to low stratospheric temperatures, Geophys. Res. Lett., 22, 247-250, 1995.

Cecil, D.J., Buechler, D. E., Blakeslee, R. J. : Gridded lightning climatology from TRMM-LIS and OTD: Dataset description, Atmospheric Research, 135–136, 404-414, doi:10.1016/j.atmosres.2012.06.028, 2012.

Chin, M., D. J. Jacob, G. M. Gardner, M. S. Foreman-Fowler, P. A. Spiro, and D. L. Savoie: A global three-dimensional model of tropospheric sulfate, J. Geophys. Res., 101, (D13), 18,667–18,690, 1996

Christian, H. J., et al. (2003), Global frequency and distribution of lightning as observed from space by the Optical Transient Detector, J. Geophys. Res., 108(D1), 4005, doi:10.1029/2002JD002347.

Dee, D.P., Uppala, S.M., Simmons, A.J., Berrisford, P., Poli, P., Kobayashi, S., Andrae, U., Balmaseda, M.A., Balsamo, G., Bauer, P., Bechtold, P., Beljaars, A.C.M., van de Berg, L., Bidlot, J., Bormann, N., Delsol, C., Dragani, R., Fuentes, M., Geer, A.J., Haimberger, L., Healy, S.B., Hersbach, H., Hólm, E.V., Isaksen, L., Kållberg, P., Köhler, M., Matricardi, M., Mcnally, A.P., Monge-Sanz, B.M., Morcrette, J.-J., Park, B.-K., Peubey, C., de Rosnay, P., Tavolato, C., Thépaut, J.-N., Vitart, F.The ERA-Interim reanalysis: Configuration and performance of the data assimilation system, Quarterly Journal of the Royal Meteorological Society, 2011.

Deeter, M. N., S. Martínez-Alonso, D. P. Edwards, L. K. Emmons, J. C. Gille, H. M. Worden, J. V. Pittman, B. C. Daube, and S. C. Wofsy: Validation of MOPITT Version 5 thermal-infrared, near-infrared, and multispectral carbon monoxide profile retrievals for 2000–2011, J. Geophys. Res. Atmos., 118, 6710–6725, doi:10.1002/jgrd.50272, 2013a.

Deeter, M.N., MOPITT Version 6 Product User's Guide, Technical Report, NCAR, Boulder, USA, 2013.137 (656), pp. 553-597, 2013b.

Diamantakis, M. and Flemming, J.: Global mass fixer algorithms for conservative tracer transport in the ECMWF model, Geosci. Model Dev., 7, 965-979, doi:10.5194/gmd-7-965-2014, 2014.

Elguindi, N., Clark, H., Ordóñez, C., Thouret, V., Flemming, J., Stein, O., Huijnen, V., Moinat, P., Inness, A., Peuch, V.-H., Stohl, A., Turquety, S., Athier, G., Cammas, J.-P., and Schultz, M.: Current status of the ability of the GEMS/MACC models to reproduce the tropospheric CO vertical distribution as measured by MOZAIC, Geosci. Model Dev., 3, 501-518, doi:10.5194/gmd-3-501-2010, 2010.

Emmons, L. K., Walters, S., Hess, P. G., Lamarque, J.-F., Pfister, G. G., Fillmore, D., Granier, C., Guenther, A., Kinnison, D., Laepple, T., Orlando, J., Tie, X., Tyndall, G., Wiedinmyer, C., Baughcum, S. L., and Kloster, S.: Description and evaluation of the Model for Ozone and Related chemical Tracers, version 4 (MOZART-4), Geosci. Model Dev., 3, 43-67, doi:10.5194/gmd-3-43-2010, 2010.

Emmons, L.K. et al: The POLARCAT Model Intercomparison Project (POLMIP): Overview and evaluation with observations, Atmospheric Chemistry and Physics, to be submitted, 2014.

Engelen, R. J., Serrar, S., and Chevallier, F.: Four-dimensional data assimilation of atmospheric CO2 using AIRS observations, J. Geophys. Res., 114, D03303, doi:10.1029/2008JD010739, 2009.

Errera, Q., Daerden, F., Chabrillat, S., Lambert, J. C., Lahoz, W. A., Viscardy, S., Bonjean, S., and Fonteyn, D.: 4D-Var assimilation of MIPAS chemical observations: ozone and nitrogen dioxide analyses, Atmos. Chem. Phys., 8, 6169-6187, doi:10.5194/acp-8-6169-2008, 2008.

Fiore, A.M., Naik, V., Spracklen, D.V., Steiner, A., Unger, N., Prather, M., Bergmann, D., Cameron-Smith, P.J., Cionni, I., Collins, W.J., Dalsoren, S., Eyring, V., Folberth, G.A., Ginoux, P., Horowitz, L.W., Josse, B., Lamarque, J.-F., MacKenzie, I.A., Nagashima, T., O'Connor, F.M., Righi, M., Rumbold, S.T., Shindell, D.T., Skeie, R.B., Sudo, K., Szopa, S., Takemura, T., Zeng, G., Global air quality and climate, Chemical Society Reviews, 41 (19), pp. 6663-6683, 2012.

Flemming, J., Stern, R., and Yamartino, R. J.: A new air quality regime classification scheme for O_3, NO_2, SO_2 and PM10 observations sites, Atmos. Environ., 39, 6121–6129, 2005

Flemming, J., Inness, A., Flentje, H., Huijnen, V., Moinat, P., Schultz, M. G., and Stein, O.: Coupling global chemistry transport models to ECMWF's integrated forecast system, Geosci. Model Dev., 2, 253-265, doi:10.5194/gmd-2-253-2009, 2009 a.

Flemming, J., Inness, A., Flentje, H., Huijnen, V., Moinat, P., Schultz, M. G., and Stein, O. ECMWF technical memorandum 590 [http://old.ecmwf.int/publications/library/ecpublications/_pdf/tm/501-600/tm590.pdf] tm590.pdf, 2009 b.

Flemming, J., Inness, A., Jones, L., Eskes, H. J., Huijnen, V., Schultz, M. G., Stein, O., Cariolle, D., Kinnison, D., and Brasseur, G.: Forecasts and assimilation experiments of the Antarctic ozone hole 2008, Atmos. Chem. Phys., 11, 1961–1977, doi:10.5194/acp-11-1961-2011, 2011 a.

Flemming, J. and Huijnen, V.: IFS Tracer Transport Study, MACC Deliverable G-RG 4.2, Tech. rep., ECMWF, http://www.gmes-atmosphere.eu/documents/deliverables/g-rg/ifs transport study.pdf, 2011 b.

Flemming, J.; Peuch, V.-H.; Engelen, R.; Kaiser, J.W. A European Global-to-Regional Air Pollution Forecasting System that Combines Modeling with Satellite Observations; EM Magazine of A&WMA, November 2013, pp. 6-10. https://www.researchgate.net/publication/259535688_A_European_Global-to-Regional_Air_Pollution_Forecasting_System_that_Combines_Modeling_with_Satellite_Observations, 2013

Forbes, R.M., A.M. Tompkins & A. Untch, A new prognostic bulk-microphysics scheme for the IFS. ECMWF Tech. Memo. No. 649, 2011.

Fu, Q., Yang, P. and Sun, W. B.:. An accurate parametrization of the infrared radiative properties of cyrrus clouds of climate models. J. Climate, 11, 2223–2237, 1998

Gauss, M., Isaksen, I. S. A., Lee, D. S., and Søvde, O. A.: Impact of aircraft NOx emissions on the atmosphere – tradeoffs to reduce the impact, Atmos. Chem. Phys., 6, 1529-1548, doi:10.5194/acp-6-1529-2006, 2006.

Gery, M., Whitten, G. Z., Killus, J. P., and Dodge, M. C.: A photochemical kinetics mechanism for urban and regional scale computer modelling, J. Geophys. Res., 94, 18925–18956, 1989.

Giodarno, L. et al.: Assessment of the MACC/IFS-MOZART model and its influence as chemical boundary conditions in AQMEII phase 2, submitted to Atmospheric Environment.

Granier, C., J.F. Lamarque, A. Mieville, J.F. Muller, J. Olivier, J. Orlando, J. Peters, G. Petron, G. Tyndall, S. Wallens, POET, a database of surface emissions of ozone precursors, available on internet at http://www.aero.jussieu.fr/projet/ACCENT/POET.php, 2005.

Granier, C., B. Bessagnet, T. Bond, A. D'Angiola, H.D.v.d. Gon, G.J. Frost, A. Heil, J.W. Kaiser, S. Kinne, Z. Klimont, S. Kloster, J.-F. Lamarque, C. Liousse, T. Masui, F. Meleux, A. Mieville, T. Ohara, J.-C. Raut, K. Riahi, M.G. Schultz, S.J. Smith, A. Thomson, J.v. Aardenne, G.R.v.d. Werf, and D.P.v. Vuuren, Evolution of anthropogenic and biomass burning emissions of air pollutants at global and regional scales during the 1980-2010 period, Climatic Change, 109(1-2), 163-190, doi:10.1007/s10584-011-0154-1, 2011.

Grell, G. A., Peckham, S. E., Schmitz, R, McKeen, S. A.,. Frost, G. J, Skamarock, W. and Eder B.: Fully coupled online chemistry within the WRF model, Atmospheric Environment, 39, 37, 6957-6975, 2005.

Grooß, J.-U. and Russell III, J. M.: Technical note: A stratospheric climatology for O3, H2O, CH4, NOx, HCl and HF derived from HALOE measurements, Atmos. Chem. Phys., 5, 2797–2807, doi:10.5194/acp-5-2797-2005, 2005

Guenther, A. B., Karl, T., Harley, P., Wiedinmyer, C., Palmer, P. I., and Geron, C.: Estimates of global terrestrial isoprene emissions using MEGAN (Model of Emissions of Gases and Aerosols from Nature), Atmos. Chem. Phys., 6, 3181–3210, doi:10.5194/acp-6-3181-2006, 2006.

Haywood, J. M., Roberts, D. L., Slingo, A., Edwards, J. M., and Shine, K. P.: General circulation model calculations of the direct radiative forcing by anthropogenic sulfate and fossil-fuel soot aerosol, Journal of Climate, 10, 1562–1577, 1997.

Hertel, O., Berkowicz, R., Christensen, J. and Hov Ø: Test of two numerical schemes for use in atmospheric transport-chemistry models Atmos. Environ., 27A(16), 2591–2611, 1993.

Hollingsworth, A., Engelen, R.J., Textor, C., Benedetti, A., Boucher, O., Chevallier, F., Dethof, A., Elbern, H., Eskes, H., Flemming, J., Granier, C., Kaiser, J.W., Morcrette, J.-J., Rayner, P., Peuch, V.H., Rouil, L., Schultz, M.G.,. Simmons, A.J and The GEMS Consortium: Toward a Monitoring and Forecasting System For Atmospheric Composition: The GEMS Project. Bull. Amer. Meteor. Soc., 89, 1147-1164, 2008.

Holtslag, A.A. and B. Boville: Local versus nonlocal boundary-layer diffusion in a global climate model, J. Clim., 6, 1825-1842, 1993.

Horowitz, L. W., Walters, S., Mauzerall, D. L., Emmons, L. K., Rasch, P. J., Granier, C., Tie, X., Lamarque, J.-F., Schultz, M. G., Tyndall, G. S., Orlando, J. J., and Brasseur, G. P.: A global simulation of tropospheric ozone and related tracers, Description and Evaluation of MOZART version 2, J. Geophys. Res., 108, 4784, doi:10.1029/2002JD002853, 2003.

Hortal, M. and Simmons, A. J.: Use of reduced Gaussian grids in spectral models, Mon. Weather Rev., 119, 1057 1074, 1991.

Hortal, M.: The development and testing of a new two-time-level semi-Lagrangian scheme (SETTLS) in the ECMWF forecast model, 128, 1671–1687, DOI: 10.1002/qj.200212858314, 2002.

Houweling, S., Dentener, F. J., and Lelieveld, J.: The impact of nonmethane hydrocarbon compounds on tropospheric photochemistry, J. Geophys. Res., 103(D9), 10673–10696, 1998.

Huijnen, V., Williams, J., van Weele, M., van Noije, T., Krol, M., Dentener, F., Segers, A., Houweling, S., Peters, W., de Laat, J., Boersma, F., Bergamaschi, P., van Velthoven, P., Le Sager, P., Eskes, H., Alkemade, F., Scheele, R., Nédélec, P., and Pätz, H.-W.: The global chemistry transport model TM5: description and evaluation of the tropospheric chemistry version 3.0, Geosci. Model Dev., 3, 445-473, doi:10.5194/gmd-3-445-2010.

Huijnen, V., Flemming, J., Kaiser, J. W., Inness, A., Leitão, J., Heil, A., Eskes, H. J., Schultz, M. G., Benedetti, A., Hadji-Lazaro, J., Dufour, G., and Eremenko, M.: Hindcast experiments of tropospheric composition during the summer 2010 fires over western Russia, Atmos. Chem. Phys., 12, 4341-4364, doi:10.5194/acp-12-4341-2012, 2012.

Huijnen, V., Williams, J. E., and Flemming, J.: Modeling global impacts of heterogeneous loss of HO2 on cloud droplets, ice particles and aerosols, Atmos. Chem. Phys. Discuss., 14, 8575-8632, doi:10.5194/acpd-14-8575-2014, 2014.

Im, U. et al.: Evaluation of operational online-coupled regional air quality models over Europe and North America in the context of AQMEII phase 2. Part I: Ozone, submitted to Atmospheric Environment.

Inness, A., Baier, F., Benedetti, A., Bouarar, I., Chabrillat, S., Clark, H., Clerbaux, C., Coheur, P., Engelen, R. J., Errera, Q., Flemming, J., George, M., Granier, C., Hadji-Lazaro, J., Huijnen, V., Hurtmans, D., Jones, L., Kaiser, J. W., Kapsomenakis, J., Lefever, K., Leitão, J., Razinger, M., Richter, A., Schultz, M. G., Simmons, A. J., Suttie, M., Stein, O., Thépaut, J.-N., Thouret, V., Vrekoussis, M., Zerefos, C., and the MACC team: The MACC reanalysis: an 8 yr data set of atmospheric composition, Atmos. Chem. Phys., 13, 4073-4109, doi:10.5194/acp-13-4073-2013, 2013.

Jacob, D.J. H. Liu, C.Mari, and R.M. Yantosca, Harvard wet deposition scheme for GMI, Harvard University Atmospheric Chemistry Modeling Group, revised March 2000. http://acmg.seas.harvard.edu/geos/wiki_docs/deposition/wetdep.jacob_etal_2000.pdf

Jakob, C. and Klein, S.: A parameterization of the effects of cloud and precipitation overlap for use in general-circulation models, Q. J. Roy. Meteor. Soc., 126, 2525–2544, 2000.

Jung, T., T. N. Palmer, M. J. Rodwell, and S. Serrar, 2008: Diagnosing forecast error using relaxation experiments. ECMWF Newsletter 82, ECMWF, Shinfield Park, Reading, Berkshire RG2 9AX, UK.

Kaiser, J. W., Heil, A., Andreae, M. O., Benedetti, A., Chubarova, N., Jones, L., Morcrette, J.-J., Razinger, M., Schultz, M. G., Suttie, M., and van der Werf, G. R.: Biomass burning emissions estimated with a global fire assimilation system based on observed fire radiative power, Biogeosciences, 9, 527-554, doi:10.5194/bg-9-527-2012, 2012.

Kaminski, J. W., Neary, L., Struzewska, J., McConnell, J. C., Lupu, A., Jarosz, J., Toyota, K., Gong, S. L., Côté, J., Liu, X., Chance, K., and Richter, A.: GEM-AQ, an on-line global multiscale chemical weather modelling system: model description and evaluation of gas phase chemistry processes, Atmos. Chem. Phys., 8, 3255-3281, 2008.

Kinnison, D. E., Brasseur, G. P., Walters, S., Garcia, R. R.,. Marsh, D. R, Sassi, F., Harvey, V. L., Randall, C. E., Emmons, L., Lamarque, J. F., Hess, P., Orlando, J. J., Tie, X. X., Randel, W., Pan, L. L., Gettelman, A., Granier, C., Diehl, T., Niemeier, U. and Simmons, A. J.: Sensitivity of Chemical Tracers to Meteorological Parameters in the MOZART-3 Chemical Transport Model. J. Geophys. Res, 112, D03303, doi:10.1029/2008JD010739,2007.

Komhyr, W. D., Barnes, R. A., Borthers, G. B., Lathrop, J. A., Kerr, J. B., and Opperman, D. P.: Electrochemical concentration cell ozonesonde performance evaluation during STOIC 1989, J. Geophys. Res., 100, 9231–9244, 1995

Lamarque, J.-F., Emmons, L. K., Hess, P. G., Kinnison, D. E., Tilmes, S., Vitt, F., Heald, C. L., Holland, E. A., Lauritzen, P. H., Neu, J., Orlando, J. J., Rasch, P. J., and Tyndall, G. K.: CAM-chem: description and evaluation

of interactive atmospheric chemistry in the Community Earth System Model, Geosci. Model Dev., 5, 369-411, doi:10.5194/gmd-5-369-2012, 2012.

Landgraf, J. and Crutzen, P. J.: An efficient method for online calculations of photolysis and heating trates, J. Atmos. Sci., 55, 863–878, 1998.

Lawrence, M.G. and Crutzen, P. J: The impact of cloud particle gravitational settling on soluble trace gas distributions. Tellus B, 50: 263–289. doi: 10.1034/j.1600-0889.1998.

Lefever, K., van der A, R., Baier, F., Christophe, Y., Errera, Q., Eskes, H., Flemming, J., Inness, A., Jones, L., Lambert, J.-C., Langerock, B., Schultz, M. G., Stein, O., Wagner, A., and Chabrillat, S.: Copernicus atmospheric service for stratospheric ozone: validation and intercomparison of four near real-time analyses, 2009–2012, Atmos. Chem. Phys. Discuss., 14, 12461-12523, doi:10.5194/acpd-14-12461-2014, 2014.

Lin, J.-T., McElroy, M. B., and Boersma, K. F.: Constraint of anthropogenic NOx emissions in China from different sectors: a new methodology using multiple satellite retrievals, Atmos. Chem. Phys., 10, 63-78, doi:10.5194/acp-10-63-2010, 2010.

Liu, H., Jacob, D.J., Bey, I., Yantosca, R.M., 2001. Constraints from 210 Pb and 7 Be on wet deposition and transport in a global three-dimensional chemical tracer model driven by assimilated meteorological fields. Journal of Geophysical Research 106, 12109e12128.

McGregor, J. L.: C-CAM Geometric Aspects and Dynamical Formulation, Tech. Rep. 70, CSIRO Atmospheric Research, Aspendale, Victoria, 2005.

MACC VAL report, Validation report of the MACC reanalysis of global atmospheric composition Period, 2003-2011.http://www.copernicusatmosphere.eu/documents/maccii/deliverables/val/MACCII_VAL_DEL_D_83.4_REAreport02_20130207.pdf, 2013

Mann, G. W., Carslaw, K. S., Spracklen, D. V., Ridley, D. A., Manktelow, P. T., Chipperfield, M. P., Pickering, S. J., and Johnson, C. E.: Description and evaluation of GLOMAP-mode: a modal global aerosol microphysics model for the UKCA composition-climate model, Geosci. Model Dev., 3, 519-551, doi:10.5194/gmd-3-519-2010, 20103-651-2010, 2010.

Marenco, A., Thouret, V., Ńedelec, P., Smit, H. G., Helten, M., Kley, D., Karcher, F., Simon, P., Law, K., Pyle, J., Poschmann, G., Von Wrede, R., Hume, C., and Cook, T.: Measurement of ozone and water vapour by Airbus in-service air-craft: The MOZAIC airborne programme, an overview, J. Geophys. Res., 103, 25631–25642, 1998.

Mari, C., Jacob, D. J., and Bechtold, P.: Transport and scavenging of soluble gases in a deep convective cloud, J. Geophys. Res., 105, 22 255-22 267, 2000.

Matsumi, Y., Comes, F. J., Hancock, G., Hofzumahus, A., Hynes, A. J., Kawasaki, M., and Ravishankara, A. R.: Quantum yields for the production of O(1D) in the ultraviolet photolysis of ozone: recommendation based on evaluation of laboratory data, J. Geophys. Res., 107, 4024, doi:10.1029/2001JD000510, 2002.

Meijer, E.W., P. F. J. van Velthoven, D. W. Brunner, H. Huntrieser and H. Kelder: Improvement and evaluation of the parameterization of nitrogen oxide production by lightning, Physics and Chemistry of the Earth, Part C, Volume 26, Issue 8, Pages 577-583, 2001.

Ménard, R. et al.,Coupled chemical-dynamical data assimilation, Final Report, ESA/ESTEC. 2007.

Metzger, S., F. Dentener, S. Pandis, and J. Lelieveld, Gas/aerosol partitioning, 1, A computationally efficient model, J. Geophys. Res., 107(D16), doi:10.1029/2001JD001102, 2002a.

Metzger, S., Dentener, F., Krol, M. C., Jeuken, A., and Lelieveld, J.: Gas/aerosol partitioning 2. Global modeling results, J. Geophys. Res., 107(D16), 4313, doi:10.1029/2001JD001103, 2002b.

Morcrette, J.-J., Boucher, O., Jones, L., Salmond, D., Bechtold, P., Beljaars, A., Benedetti, A., Bonet, A., Kaiser, J. W., Razinger, M., Schulz, M., Serrar, S., Simmons, A. J., Sofiev, M., Suttie, M., Tompkins, A. M. and Untch, A.: Aerosol analysis and forecast in the ECMWF Integrated Forecast System. Part I: Forward modelling, J. Geophys. Res., 2009.

Morgenstern, O., Braesicke, P., O'Connor, F. M., Bushell, A. C., Johnson, C. E., Osprey, S. M., and Pyle, J. A.: Evaluation of the new UKCA climate-composition model – Part 1: The stratosphere, Geosci. Model Dev., 2, 43–57, doi:10.5194/gmd-2-43-2009, 2009.

Michou M., P. Laville, D. Serça, A. Fotiadi, P. Bouchou and V.-H. Peuch, Measured and modeled dry deposition velocities over the ESCOMPTE area, Atmos. Res., 74 (1-4), 89-116, 2004.

Nedelec, P., Cammas, J.-P., Thouret, V., Athier, G., Cousin, J.-M., Legrand, C., Abonnel, C., Lecoeur, F., Cayez, G., and Marizy, C.: An improved infrared carbon monoxide analyser for routine measurements aboard commercial Airbus aircraft: technical validation and first scientific results of the MOZAIC III programme, Atmos. Chem. Phys., 3, 1551–1564, doi:10.5194/acp-3-1551-2003, 2003.

Neu, J. L. and Prather, M. J.: Toward a more physical representation of precipitation scavenging in global chemistry models: cloud overlap and ice physics and their impact on tropospheric ozone, Atmos. Chem. Phys., 12, 3289-3310, doi:10.5194/acp-12-3289-2012, 2012.

O'Connor, F. M., Johnson, C. E., Morgenstern, O., Abraham, N. L., Braesicke, P., Dalvi, M., Folberth, G. A., Sanderson, M. G., Telford, P. J., Voulgarakis, A., Young, P. J., Zeng, G., Collins, W. J., and Pyle, J. A.: Evaluation of the new UKCA climate-composition model – Part 2: The Troposphere, Geosci. Model Dev., 7, 41-91, doi:10.5194/gmd-7-41-2014, 2014.

Olivier J., J. Peters, C. Granier, G. Petron, J.F. Muller, and S. Wallens: Present and future surface emissions of atmospheric compounds, POET report #2, EU project EVK2-1999-00011, 2003

Ordóñez, C., Elguindi, N., Stein, O., Huijnen, V., Flemming, J., Inness, A., Flentje, H., Katragkou, E., Moinat, P., Peuch, V.-H., Segers, A., Thouret, V., Athier, G., van Weele, M., Zerefos, C. S., Cammas, J.-P., and Schultz, M. G.: Global model simulations of air pollution during the 2003 European heat wave, Atmos. Chem. Phys., 10, 789-815, doi:10.5194/acp-10-789-2010, 2010.

Ott, L. E., K. E. Pickering, G. L. Stenchikov, D. J. Allen, A. J. DeCaria, B. Ridley, R.-F. Lin, S. Lang, and W.-K. Tao (2010), Production of lightning NOx and its vertical distribution calculated from three-dimensional cloud-scale chemical transport model simulations, J. Geophys. Res., 115, D04301, doi:10.1029/2009JD011880.

Pickering, K. E., Y. Wang, W.-K. Tao, C. Price, and J.-F. Müller: Vertical distributions of lightning NOx for use in regional and global chemical transport models, J. Geophys. Res., 103, 31,203 – 31,216, doi:10.1029/98JD0265. 1998.

Pozzoli L., Bey, I., Rast, J. S., Schultz, M. G., Stier, P., and Feichter, J.: Trace gas and aerosol interactions in the fully coupled model of aerosol-chemistry-climate ECHAM5-HAMMOZ, PART I: Model description and insights from the spring 2001 TRACE-P experiment, J. Geophys. Res., 113, 2008.

Prather, M. J., Holmes, C. D., and Hsu, J.: Reactive greenhouse gas scenarios: Systematic exploration of uncertainties and the role of atmospheric chemistry, Geophys. Res. Lett., 39, L09803,doi:10.1029/2012GL051440, 2012.

Price, C., and Rind, D.: A simple lightning parameterization for calculating global lightning distributions, J. Geophys. Res., 9 7, 9919-9933, 1992.

Price, C., and Rind, D.: What determines the cloud-to-ground fraction in thunderstorms? Geophys Res. Lett., 20, 463-466, 1993.

Price, C., J. Penner, and M. Prather: NOx from lightning 1. Global distributions based on lightning physics, J. Geophys. Res., 102, 5929–5941, doi:10.1029/96JD03504, 1997.

Rast, S., Schultz, M.G., Bey, I., van Noije, T., Aghedo, A.M., Brasseur, G.P., Diehl, T., Esch, M., Ganzeveld, L., Kirchner, I., Kornblueh, L., Rhodin, A., Röckner, E., Schmidt, H., Schröder, S., Schulzweida, U., Stier, P., Thomas, K., Walters, S.: Evaluation of the tropospheric chemistry general circulation model ECHAM5–MOZ and its application to the analysis of the chemical composition of the troposphere with an emphasis on the late RETRO period 1990–2000, Reports on Earth-System Science, 114, Max-Planck Institut fuer Meteorologie, Hamburg, 2014.

Redler, R., Valcke, S. and Ritzdorf, H.: OASIS4 - A Coupling Software for Next Generation Earth System Modelling, Geoscience Model Development, 3, 87 - 104, DOI:10.5194/gmd-3-87-2010.

Richter, A., Burrows, J. P., Nüß, H., Granier, C, Niemeier, U., Increase in tropospheric nitrogen dioxide over China observed from space, Nature, 437, 129-132, doi: 10.1038/nature04092, 2005.

Sander, R., Compilation of Henry's Law Constants for Inorganic and Organic Species of Potential Importance in Environmental Chemistry, MPI for Chemistry Mainz, Germany, 1999, http://www.henrys-law.org/henry.pdf

Sander, S.P., et al., Chemical Kinetics and Photochemical Data for Use in Atmospheric Studies, Evaluation Number 14, JPL Publication 02-25, Jet Propulsion Laboratory, Pasadena, Calif., 2003.

Sander, S.P., et al., Chemical Kinetics and Photochemical Data for Use in Atmospheric Studies, Evaluation Number 15, JPL Publication 06-02, Jet Propulsion Laboratory, Pasadena, Calif., 2006.

Sander, S. P., Abbatt, J. R., Burkholder, J. B., Friedl, R. R., Golden, D. M., Huie, R. E., Kolb, C. E., Kurylo, G., Moortgat, K., Orkin, V. L. and Wine, P. H.: Chemical kinetics and Photochemical Data for Use in Atmospheric studies, Evaluation No.17, JPL Publication 10-6, Jet Propulsion Laboratory, Pasadena, 2011.

Schumann, U., and H. Huntrieser: The global lightning-induced nitrogen oxides source, Atmos. Chem. Phys., 7, 3823–3907, 2007.

Seinfeld J. H. and Pandis S. N., Atmospheric Chemistry and Physics: From Air Pollution to Climate Change, 1st edition, J. Wiley, New York, 1998.

Shindell, D.T., G. Faluvegi, D.S. Stevenson, M.C. Krol, L.K. Emmons, J.-F. Lamarque, G. Pétron, F.J. Dentener, K. Ellingsen, M.G. Schultz, O. Wild, M. Amann, C.S. Atherton, D.J. Bergmann, I. Bey, T. Butler, J. Cofala, W.J. Collins, R.G. Derwent, R.M. Doherty, J. Drevet, H.J. Eskes, A.M. Fiore, M. Gauss, D.A. Hauglustaine, L.W. Horowitz, I.S.A. Isaksen, M.G. Lawrence, V. Montanaro, J.-F. Müller, G. Pitari, M.J. Prather, J.A. Pyle, S. Rast, J.M. Rodriguez, M.G. Sanderson, N.H. Savage, S.E. Strahan, K. Sudo, S. Szopa, N. Unger, T.P.C. van Noije, and G. Zeng: Multi-model simulations of carbon monoxide: Comparison with observations and projected near-future changes. J. Geophys. Res., 111, D19306, doi:10.1029/2006JD007100, 2006.

Slingo, A.: A GCM parameterization for the shortwave radiative properties of water clouds. J. Atmos. Sci., 46, 1419–1427, 1989.

Smithson, P. A., IPCC, 2001: climate change 2001: the scientific basis. Contribution of Working Group 1 to the Third Assessment Report of the Intergovernmental Panel on Climate Change, edited by J. T. Houghton, Y. Ding, D. J. Griggs, M. Noguer, P. J. van der Linden, X. Dai, K. Maskell and C. A. Johnson (eds). Cambridge University Press, Cambridge, UK, and New York, USA, Int. J. Climatol., 22: 1144. doi: 10.1002/joc.763, 2002.

Steil, B., Dameris, M., Brühl, C., Crutzen, P. J., Grewe, V., Ponater, M., and Sausen, R.: Development of a chemistry module for GCMs: first results of a multiannual integration, Ann. Geophys., 16, 205-228, doi:10.1007/s00585-998-0205-8, 1998.

Stein, O., Flemming, J., Inness, A., Kaiser, J.W., Schultz, M.G., Global reactive gases forecasts and reanalysis in the MACC project, Journal of Integrative Environmental Sciences, 9, Iss. sup1, 57-70, doi:10.1080/1943815X.2012.696545, 2012.

Stein, O., Schultz, M. G., Bouarar, I., Clark, H., Huijnen, V., Gaudel, A., George, M., and Clerbaux, C.: On the wintertime low bias of Northern Hemisphere carbon monoxide in global model studies, Atmos. Chem. Phys. Discuss., 14, 245-301, doi:10.5194/acpd-14-245-2014, 2014.

Steinbrecht, W., Shwartz, R., and Claude, H.: New pump correction for the Brewer-Mast ozone sonde: Determination from experiment and instrument intercomparisons, J. Atmos. Ocean. Tech.15, 144–156, 1998.

Stevenson, D. S., et al. (2006), Multimodel ensemble simulations of present-day and near-future tropospheric ozone, J. Geophys. Res., 111, D08301, doi:10.1029/2005JD006338.

Temperton, C., Hortal, M. and Simmons, A.: A two-time-level semi-Lagrangian global spectral model, QJR, 127, 111-127, 2001.

Tiedtke, M. A: comprehensive mass flux scheme for cumulus parameterization in large-scale models. Mon. Weather. Rev., 117(8):1779-1800, 1989.

Wesely, M.L.: Parameterization of Surface Resistances to Gaseous Dry Deposition in Regional-Scale Numerical Models. Atmos. Environ., 23, 1293-1304, 1989.

von Blohn, N., Diehl, K., Mitra, S. K., and Borrmann, S.: Wind tunnel experiments on the retention of trace gases during riming: nitric acid, hydrochloric acid, and hydrogen peroxide, Atmos. Chem. Phys., 11, 11569-11579, doi:10.5194/acp-11-11569-2011, 2011.

van Noije, T. P. C., Le Sager, P., Segers, A. J., van Velthoven, P. F. J., Krol, M. C., and Hazeleger, W.: Simulation of tropospheric chemistry and aerosols with the climate model EC-Earth, Geosci. Model Dev. Discuss., 7, 1933-2006, doi:10.5194/gmdd-7-1933-2014, 2014.

Voulgarakis, A., Naik, V., Lamarque, J.-F., Shindell, D. T., Young, P. J., Prather, M. J., Wild, O., Field, R. D., Bergmann, D., Cameron-Smith, P., Cionni, I., Collins, W. J., Dalsøren, S. B., Doherty, R. M., Eyring, V., Faluvegi, G., Folberth, G. A., Horowitz, L. W., Josse, B., MacKenzie, I. A., Nagashima, T., Plummer, D. A., Righi, M., Rumbold, S. T., Stevenson, D. S., Strode, S. A., Sudo, K., Szopa, S., and Zeng, G.: Analysis of present day and future OH and methane lifetime in the ACCMIP simulations, Atmos. Chem. Phys., 13, 2563-2587, doi:10.5194/acp-13-2563-2013, 2013.

Williams, J. E., Strunk, A., Huijnen, V., and van Weele, M.: The application of the Modified Band Approach for the calculation of on-line photodissociation rate constants in TM5: implications for oxidative capacity, Geosci. Model Dev., 5, 15-35, doi:10.5194/gmd-5-15-2012, 2012.

Williams, J. E., van Velthoven, P. F. J., and Brenninkmeijer, C. A. M.: Quantifying the uncertainty in simulating global tropospheric composition due to the variability in global emission estimates of Biogenic Volatile Organic 2857-2013, 2013.

Wittrock, F., A. Richter, H. Oetjen, J. P. Burrows, M. Kanakidou, S. Myriokefalitakis, R. Volkamer, S. Beirle, U. Platt, and T. Wagner, Simultaneous global observations of glyoxal and formaldehyde from space, Geophys. Res. Lett., 33, L16804, doi:10.1029/2006GL026310, 2006Compounds, Atmos. Chem. Phys., 13, 2857-2891, doi:10.5194/acp-13-2857-2013, 2013.

Yarwood, G., Rao, S., Yocke, M., and Whitten, G.: Updates to the carbon bond chemical mechanism: CB05. Final report to the US EPA, EPA Report Number: RT-0400675, available at: www.camx.com, last access: 1 July 2014, 2005.

WMO (2007), WMO Global Atmosphere Watch (GAW) Strategic Plan: 2008 – 2015. World Meteorological Organization, Geneva, Switzerland, 2007.

Young, P. J., Archibald, A. T., Bowman, K. W., Lamarque, J.-F., Naik, V., Stevenson, D. S., Tilmes, S., Voulgarakis, A., Wild, O., Bergmann, D., Cameron-Smith, P., Cionni, I., Collins, W. J., Dalsøren, S. B., Doherty, R. M., Eyring, V., Faluvegi, G., Horowitz, L. W., Josse, B., Lee, Y. H., MacKenzie, I. A., Nagashima, T., Plummer, D. A., Righi, M., Rumbold, S. T., Skeie, R. B., Shindell, D. T., Strode, S. A., Sudo, K., Szopa, S., and Zeng, G.: Pre-industrial to end 21st century projections of tropospheric ozone from the Atmospheric Chemistry and Climate Model Intercomparison Project (ACCMIP), Atmos. Chem. Phys., 13, 2063-2090, doi:10.5194/acp-13-2063-2013, 2013.

Zaveri, R. A. and Peters, L. K.: A new lumped structure photochemical mechanism for large-scale applications, J. Geophys. Res., 104, 30387–30415, doi:10.1029/1999JD900876, 1999.

Zdunkowski, W. G., Welsch, R. M., and Kord, G. J.: An investigation of the structure of typical 2-stream methods for the calculation of solar fluxes and heating rates in clouds, Contrib. Atmos. Phys., 53, 215–238, 1980.

Zhang, L., Brook, J. R., and Vet, R.: A revised parameterization for gaseous dry deposition in air-quality models, Atmos. Chem. Phys., 3, 2067-2082, doi:10.5194/acp-3-2067-2003, 2003.

Zhang, Y.: On-line coupled meteorology and chemistry models: history, current status, and outlook, Atmos. Chem. Phys, 8, 2895-2032, 2008.

Supplement

Short name	Long name	Dry Depo-sition	Wet Depo-sition	Molar Mass (g/mol)	H_A (M / atm)	ΔH_A *(kcal / mol)*
O3	ozone	yes	no	48	0	0
H2O2	hydrogen peroxide	yes	yes	34	8.30E+04	7400
CH4	methane	no	no	16	0	0
CO	carbon monoxide	yes	yes	28	9.90E-04	1300
HNO3	nitric acid	yes	yes	63	3.20E+11	8700
CH3OOH	methylperoxide	yes	yes	48	3.10E+02	5200
HCHO	formaldehyde	yes	yes	30	3.20E+03	6800
PAR	paraffins	no	no	12	0	0
C2H4	ethene	no	no	28	0	0
OLE	olefins	no	no	24	0	0
ALD2	aldehydes	true	yes	24	17	5000
PAN	peroxyacetyl nitrate	yes	yes	121	8.00E+00	6500
ROOH	peroxides	yes	yes	47	340	6000
ONIT	organic nitrates	yes	yes	77	7.50E+03	6485
C5H8	isoprene	no	no	68.1	0	0
SO2	sulfur dioxide	yes	yes	64.1	1.00E+05	3000
DMS	dimethyl sulfide	no	no	62.1	0	0
NH3	ammonia	yes	yes	17	75	3400
SO4	sulfate	yes	yes	96.1	3.20E+11	8700
NH4	ammonium	no	yes	18	3.20E+11	8700
MSA	methanesulfonic acid	no	yes	96.1	3.20E+11	8700
CH3COCHO	methylglyoxal	true	true	72.1	3.20E+04	8700
O3S	stratospheric ozone	true	no	48	0	0

Rn	radon	no	no	222	0	0
Pb	lead	no	yes	210	3.20E+11	8700
NO	nitrogen monoxide	yes	yes	30	1.90E-03	1400
HO2	hydroperoxy radical	no	yes	33	4.00E+03	5900
CH3O2	methylperoxy radical	no	no	47	0	0
OH	hydroxyl radical	no	no	17	0	0
NO2	nitrogen dioxide	true	yes	46	1.20E-02	2500
NO3	nitrate radical	yes	yes	62	2.00E+00	2000
N2O5	dinitrogen pentoxide	yes	yes	76	2.10E+01	3400
HO2NO2	pernitric acid	yes	yes	79	1.20E+04	6900
C2O3	peroxyacetyl radical	no	no	75	0	0
ROR	organic ethers	no	no	28	0	0
RXPAR	PAR budget corrector	no	no	12	0	0
XO2	NO to NO2 operator	no	no	44	0	0
XO2N	NO to alkyl nitrate operator	no	no	44	0	0
NH2	amine	no	no	16	0	0
PSC	polar stratosph cloud	no	no	1	0	0
CH3OH	methanol	yes	yes	31.01	220	5200
HCOOH	formic acid	true	true	46.01	8.90E+03	6100
MCOOH	methacrylic acid	true	true	62.02	4.10E+03	6300
C2H6	ethane	no	no	30.02	0	0
C2H5OH	ethanol	yes	yes	46.02	190	6600
C3H8	propane	no	no	44.03	0	0
C3H6	propene	no	no	42.03	0	0
C10H16	terpenes	no	no	136	0	0
ISPD	methacrolein MVK	yes	no	70	0	0

NO3 A	nitrate	true	yes	62	3.20E+11	8700
CH3COCH3	acetone	no	true	58	35	3800
ACO2	acetone product	no	no	58	0	0
IC3H7O2	IC3H7O2	no	no	75	0	0
HYPROPO2	HYPROPO2	no	no	91	0	0

Table A1 Species of CB05 in C-IFS, if subject to wet and dry deposition and the Henry's law coefficicnet (H_A) and Heat of Dissolution (ΔH_A) at 298 K

Reactants	Products	Rate Expression	Reference
$NO + O_3$	NO_2	3.0E-12*exp(-1500/T)	[1]
$NO + HO_2$	$NO_2 + OH$	3.5E-12*exp(250/T)	[1]
$NO + CH_3O_2$	$HCHO + HO_2 + NO_2$	2.8E-12*exp(300/T)	[1]
$NO_2 + OH$ (+ M)	HNO_3	$K_0 = 1.8E\text{-}30*(300/T)^{3.0}$ $K_\infty = 2.8E\text{-}11$	[1],[2]
$OH + HNO_3$	NO_3	$K_0 = 2.41E\text{-}14*(460/T)$ $K_2 = 2.29E\text{-}17*(2199/T)$ $K_3 = 6.51E\text{-}14*(1336/T)$	[1],[2]
$NO_2 + O_3$	NO_3	1.2E-13*exp(-2540/T)	[1]
$NO + NO_3$	$NO_2 + NO_2$	1.5E-11*exp(170/T)	[1]
$NO_2 + NO_3$	N_2O_5	$K_0 = 2.0E\text{-}30*(300/T)^{4.4}$ $K_\infty = 1.4E\text{-}12*(300/T)^{0.7}$	[1],[2]
N_2O_5	$NO_2 + NO_3$	2.7E-27*exp(11000/T)	[1],[2]
$OH + HNO_4$	NO_2	1.3E-12*exp(380/T)	[1],[2]
$NO_2 + HO_2$	HNO_4	$K_0 = 2.0E\text{-}31*(300/T)^{3.4}$ $K_\infty = 2.9E\text{-}12*(300/T)^{1.1}$	[1],[2]
HNO_4 (+ M)	$NO_2 + HO_2$	2.1E-27*exp(10900/T)	[1],[2]
$O(^1D)$ (+ M)		3.3E-11*exp(55/T)*[O_2] + 2.15E11*exp(110/T)*[N_2]	[1],[2]
$O(^1D) + H_2O$	OH + OH	1.63E-10*exp(60/T)	[1],[2]
$O_3 + HO_2$	OH	1.0E-14*exp(-490/T)	[1]
CO + OH	HO_2	$K_0 = 5.9E\text{-}33*(300/T)^{1.4}$ $K_\infty = 1.1E\text{-}12*(300/T)^{-1.3}$ $K_0 = 1.5E\text{-}13*(300/T)^{-0.6}$ $K_\infty = 2.1E9*(300/T)^{-6.1}$	[1],[2]
$O_3 + OH$	HO_2	1.7E-12*exp(-940/T)	[1]
$OH + H_2O_2$	HO_2	1.8E-12	[1]
OH + HCHO	$CO + HO_2$	5.5E-12*exp(125/T)	[1]
$OH + CH_4$	CH_3O_2	2.45E-12*exp(-1775/T)	[1]
$OH + CH_3OOH$	$0.7\ CH_3O_2 + 0.3$ HCHO + 0.3 OH	3.8E-12*exp(200/T)	[1]
OH + ROOH	0.77 XO_2 + 0.19 CH3COCHO + 0.04 ALD2 + 0.23 OH + RXPAR	2E-11	[4],[5]
$CH_3O_2 + HO_2$	CH_3OOH	4.1E-13*exp(750/T)	[1]
$CH_3O_2 + CH_3O_2$	1.37 HCHO + 0.74 HO_2 + 0.63 CH_3OH	9.5E-14*exp(390/T)	[2],[5]
$OH + HO_2$		4.8E-11*exp(250/T)	[1]
$HO_2 + HO_2$	H_2O_2	3.5E-13*exp(430/T) 1.77E-33*exp(1000/T) 1.4E-21*exp(2200/T)	[1],[2]
$OH + H_2$	HO_2	2.8E-12*exp(-1800/T)	[1]

NO_3 + HCHO	HNO_3 + CO + HO_2	5.8E-16	[1]
ALD2 + OH	C_2O_3	Average of : 4.4E-12*exp(365/T) 5.1E-12*exp(405/T)	[1],[6]
ALD2 + NO_3	C_2O_3 + HNO_3	Average of : 1.4E-12*exp(-1860/T) 6.4E-15	[1],[6]
NO + C_2O_3	CH_3O_2 + NO_2	8.1E-12*exp(270/T)	[1]
NO_2 + C_2O_3	PAN	K_0 = 2.7E-28*(300/T) 7.1 K_∞ = 1.2E-11*(300/T) 0.9	[3]
PAN	NO_2 + C_2O_3	K_0 = 4.9E-3*exp(-12100/T) K_∞ = 5.4E16*exp(-13830/T)	[1],[6]
NO_3 + HO_2	HNO_3	4.0E-12	[1],[3]
NO_3 + CH_3O_2	NO_2 + HO_2 + HCHO	1.2E-12	[3],[5]
NO_3 + C_2O_3	NO_2 + CH_3O_2	4.0E-12	[5]
NO_3 + XO_2	NO_2	2.5E-12	[5]
OH + CH_3OH	HCHO + HO_2	2.85E-12*exp(-345/T)	[1],[3]
OH + HCOOH	HO_2	4.0E-13	[1]
OH + C_2H_6	0.991ALD2+0.991XO2+0.009XP2N+ HO2	6.9E-12*exp(-1000/T)	[1],[6]
OH + C_2H_5OH	ALD2 + HO_2 + 0.1 XO_2 + 0.1HCHO	3.0E-12*exp(20/T)	[1],[3]
OH +CH_3COOH	CH_3O_2	4.2E-14*exp(-855/T)	[1],[6]
OH + C_3H_8	IC3H7O2	7.6E-12*exp(-585/T)	[3,11]
$IC_3H_7O_2$ + NO	0.82 CH_3COCH_3 + HO_2 +0.27 ALD2 + NO_2	4.2E-12*exp(180/T)	[11]
$IC_3H_7O_2$ + HO_2	ROOH	7.5E-13*exp(700/T)	[11]
OH + C_3H_6	HYPROPO2	ko =8.0E-27 *(-300/T)3.5 k_∞ = 3.0E-11	[3,11]
HYPROPO2 +NO	ALD2 + HCHO + HO_2 + NO_2	4.2E-12*exp(180/T)	[11]
HYPROPO2 +HO_2	ROOH	7.5E-13*exp(700/T)	[11]
O_3 + C_3H_6	0.54HCHO + 0.19HO_2 + 0.33OH + 0.56CO + 0.5ALD2 + 0.31CH_3O_2 + 0.25HCOOH	5.5E-15*exp(-1880/T)	[6,9]
NO_3 + C_3H_6	ORGNTR	4.6E-13*exp(-1155/T)	[6,9]
C_2O_3 + C_2O_3	2 CH_3O_2	2.9E-12*exp(500/T)	[1]
C_2O_3 + HO_2	0.4 CH_3COOH + 0.4 O_3	4.3E-13*exp(1040/T)	[5]
OH + PAR	0.87 XO_2 + 0.76 ROR + 0.11 HO_2 + 0.11 ALD2 + 0.11 RXPAR + 0.13 XO_2N	8.1E-13	[1],[8]
ROR	1.1 ALD2 + 0.96 XO_2 + 0.04 XO_2N + 0.02 ROR + 2.1 RXPAR + 0.94 HO_2	1E15*exp(-8000/T)	[4]
ROR	HO_2	1600.0	[1]
OH + OLE	0.8 HCHO + 0.95 ALD2 + 0.8 XO_2 + 1.57HO_2 +0.7 RXPAR + 0.62 CO	5.2E-14*exp(-610/T)	[1],[7]
O_3 + OLE	0.5 ALD2 + 0.74 HCHO + 0.76 HO_2+ 0.22 XO_2 + 0.95 CO + RXPAR + 0.1 OH	8.5E-16*exp(1520/T)	[1],[7]

NO_3 + OLE	0.91 XO_2 + HCHO + 0.09 XO_2N + NO_2 + 0.91 ALD2 + RXPAR + 0.56 HO_2 + 0.56 CO	4.6E-14*exp(400/T)	[1],[2]
OH + C_2H_4 (+M)	HO_2 + 1.56 HCHO + 0.22 ALD2 + XO_2	K_0 = 1.0E-28*(300/T) 4.5 K_∞ = 8.8E-12*(300/T) 0.85	[1],[2]
O_3 + C_2H_4	HCHO + 0.22 HO_2 + 0.12 OH + 0.24 CO + 0.52 HCOOH	1.2E-14*exp(-2630/T)	[5]
OH + CH_3COCHO	XO_2 + C_2O_3	1.5E-11	[6]
OH + TERP	1.22HO_2 + 1.25XO_2 + 0.25XO_2N + 1.22HCHO + 5.0PAR + 0.47ALD2 + 0.47CO	1.2E-11*exp(440/T)	[3],[7]
O_3 + TERP	0.57OH + 0.28HO_2 + 0.76XO_2 + 0.18XO_2N + 1.8HCHO + 0.211CO + 6.0PAR + 0.21ALD2 + 0.39C2O3 + 0.39CH3O2	6.3E-16*exp(-580/T)	[3],[7]
NO_3 + TERP	0.47NO_2 + 0.75HO_2 + 1.03XO_2 + 0.25XO_2N + 0.47ALD2 + 0.53ORGNTR + 0.47CO + 6.0PAR	1.2E-12*exp(490/T)	[3,7]
OH + ISOP	0.4 ISPD + 0. 7 XO_2 + 0.629 HCHO + 0.5 HO_2 + 0.088 XO_2N	2.7E-11*exp(390/T)	[4,12]
O_3 + ISOP	0.65 ISPD + 0.6 HCHO + 0.066 CO + 0.2 C_2O_3 + 0.15 ALD2 + 0.35 PAR + 0.066 HO_2 + 0.2 XO_2 + 0.266 OH	1.04E-14*exp(-1995/T)	[3],[7]
NO_3 + ISOP	0.2 ISPD + 0.8 HO_2 + 0.8 ORGNTR + 0.8 ALD2 + 2.4 PAR + 0.2 NO_2 + XO_2	3.15E-12*exp(-450/T)	[3],[7]
OH + ISPD	1.565PAR + 0.167HCHO + 0.503HO_2 + 0.334CO + 0.168CH_3COCHO + 0.273ALD2 + 0.498C_2O_3 + 0.713XO_2	Average of: 1.86E-11*exp(175/T) 2.6E-12*exp(610/T)	[1],[7]
O_3 + ISPD	0.114C_2O_3 + 0.15HCHO + 0.85 CH_3COCHO + 0.154HO_2 + 0.268OH + 0.064XO_2 + 0.02ALD2 + 0.36PAR + 0.225CO	Average of: 8.5E-16*exp(-1520/T) 1.4E-15*exp(-2100/T)	[3],[7]
NO_3 + ISPD	0.357ALD2 + 0.282HCHO + 1.282PAR + 0.925HO_2 + 0.643CO + 0.85ORGNTR + 0.075C_2O_3 + 0.075XO_2 + 0.15HNO_3	Average of: 6.0E-16 3.4E-15	[3],[7]
OH + CH3COCH3	ACO2	8.8E-12*exp(-1320/T)+ 1.7E-14*exp(423/T)	[3],[7]
ACO2+HO2	ROOH		[3],[7]
ACO2+CH3O2	0.5 CH3OH + 0.5HO2 +0.7ALD2 + 0.2C2O3 + 0.5CH3COCHO		[6],[7]
ACO2+NO	NO2 + C2O3 + HCHO + HO2		[6],[7]
OH + ORGNTR	NO_2 + XO_2	5.9E-13*exp(-360/T)	[7]
NO + XO_2	NO_2	2.6E-12*exp(365/T)	[1]
XO_2 + XO_2		1.6E-12*exp(-2200/T)	[1]
XO2+XO2N		6.8E-14	[1]
XO2N+XO2N		6.8E-14	[1],[6]
NO + XO_2N	ORGNTR	2.6E-12*exp(365/T)	[1]

$HO_2 + XO_2$	ROOH	7.5E-13*exp(700/T)	[1]
PAR + RXPAR		8E-11	[8]
$HO_2 + XO_2N$	ROOH	8E-12*exp(-2060/T)	[1]
DMS + OH	SO_2	1.1E-11*exp(-240/T)	[1]
DMS + OH	0.75 SO_2 + 0.25 MSA	1.0E-39*exp(5820/T) 5.0E-30*exp(6280/T)	[2]
DMS + NO_3	SO_2	1.9E-13*exp(520/T)	[10]
OH + SO_2	SO_4^{2-}	K_0 = 3.3E-31*(300/T)$^{4.3}$ K_∞ = 1.6E-12*(300/T)	[2]
OH + NH_3	NH_2	1.7E-12*exp(-710/T)	[2]
NO + NH_2		4.0E-12*exp(450/T)	[2]
$NO_2 + NH_2$		2.1E-12*exp(650/T)	[2]
$HO_2 + NH_2$		3.4E-11	[2]
$O_2 + NH_2$		6.0E-21	[2]
$O_3 + NH_2$		4.3E-12*exp(-930/T)	[2]

Table A2 The chemical mechanism as applied in C-IFS (CB05). The reaction products O_2, CO_2 and H_2O are not shown. All reactions of the NH2 radical act as sink processes for the respective radicals and oxidants. The source of the rate data is as follows: [1] Yarwood et al. (2005), [2] Sander et al. (2011), [3] IUPAC datasheet (http://iupac.pole-ether.fr), [4] Archibald et al. (2010) [5] Zaveri and Peters (1999), [6] Atkinson et al. (2006), [7] Williams et al. (2013), [8] Houweling et al. (1998), [9] Horowitz et al.(2003), [10] Atkinson et al. (2004), [11] Emmons et al. (2010), [12] Huijnen, Williams and Flemming (2014).

Stoichiometry		Reference
$O_3 + h\nu \rightarrow$	$O(^1D)$	[1,2]
$NO_2 + h\nu \rightarrow$	$NO + O_3$	[1]
$H_2O_2 + h\nu \rightarrow$	$2OH$	[1]
$HNO_3 + h\nu \rightarrow$	$OH + NO_2$	[1]
$HNO_4 + h\nu \rightarrow$	$HO_2 + NO_2$	[1]
$N_2O_5 + h\nu \rightarrow$	$NO_2 + NO_3$	[1]
$HCHO + h\nu \rightarrow$	CO	[3]
$HCHO + h\nu \rightarrow$	$CO + 2HO_2$	[3]
$CH_3OOH + h\nu \rightarrow$	$HCHO + HO_2 + OH$	[1]
$NO_3 + h\nu \rightarrow$	$NO_2 + O_3$	[1]
$NO_3 + h\nu \rightarrow$	NO	[1]
$PAN + h\nu \rightarrow$	$C_2O_3 + NO_2$	[1]
$ORGNTR + h\nu \rightarrow$	$NO_2 + 0.51\ XO_2 + 0.3ALD2 + 0.9\ HO_2 + 0.74\ C_2O_3 + 0.74\ CH_3O_2 + 1.98RXPAR$	[3]
$ALD2 + h\nu \rightarrow$	$HCHO + XO_2 + CO + 2HO_2$	[3]
$CH_3COCHO + h\nu \rightarrow$	$C_2O_3 + HO_2 + CO$	[1]
$ROOH + h\nu \rightarrow$	$OH + 0.5\ XO_2 + 0.74C_2O_3 + 0.74\ CH_3O_2 + 0.3\ ALD2 + 0.9HO_2 + 1.98\ RXPAR$	[1]
$ISPD + h\nu \rightarrow$	$0.333CO + 0.067\ ALD2 + 0.9\ HCHO + 0.832\ PAR + 1.033\ HO_2 + 0.7\ XO_2 + 0.967\ C_2O_3$	[3]
$O_2 + h\nu \rightarrow$	$2O(^3P)$	[1]
$CH_3COCH_3 + h\nu \rightarrow$	$CO + 2CH_3O_2$	[3]
$CH_3COCH_3 + h\nu \rightarrow$	$C_2O_3 + CH_3O_2$	[3]

Table A3 Photolysis reactions in as applied in C-IFS (CB05). The reaction products O_2 and H_2O are not shown. The stoichiometry of each photolytic reaction is taken from Yarwood et al. (2005) except for the photolysis of O_2. The absorbtion coefficients and quantum yields are taken from [1] Sander et al. (2011), [2] Matsumi et al. (2002) and [3] Atkinson et al. (2006). Further details are given in Williams et al., (2013).

Species	Annual Dry Deposition Loss Tg	Dry deposition time scale in days
NH3	37	1
SO2	78	3
NO3_A	6	4
ISPD	28	6
CH3COCHO	4	7
HNO3	50	7
NO2	17	8
HCHO	35	8
HCOOH	4	10
SO4	15	10
H2O2	106	10
C2H5OH	1	11
ROOH	25	16
CH3OH	74	23
ONIT	13	29
ALD2	1	30
CH3OOH	23	53
MCOOH	31	64
PAN	7	105
HO2NO2	0	110
O3	1124	121
N2O5	0	184

Table A4 Loss because of dry deposition for 2008 in Tg and as time scale in days with respect to tropospheric burden.

Species	Annual Wet Deposition Loss Tg	Wet deposition time scale in days
NO3_A	14	2
SO4	76	2
NH4	22	2
CH3COCHO	9	3
HNO3	90	4
H2O2	260	4
Pb	0	11
HCHO	22	13
ONIT	30	13
HCOOH	3	13
HO2	1	16
SO2	11	19
MCOOH	64	31
MSA	0	35
ROOH	6	68
HO2NO2	1	91
CH3OOH	10	119
C2H5OH	0	163
CH3OH	7	232
NH3	0	832

Table A5 Loss because of wet deposition for 2008 in Tg and as time scale in days with respect to tropospheric burden.